Potential of using CO_2 observations over India in regional carbon budget estimation by improving the modelling system

Vishnu Thilakan[1,2], Dhanyalekshmi Pillai[1,2], Jithin Sukumaran[1,2], Christoph Gerbig[3], Haseeb Hakkim[4], Vinayak Sinha[4], Yukio Terao[5], Manish Naja[6], and Monish Vijay Deshpande[1,2]

[1]Indian Institute of Science Education and Research Bhopal (IISERB), India.
[2]Max Planck Partner Group (IISERB), Max Planck Society, Munich, Germany
[3]Max Planck Institute for Biogeochemistry, Jena, Germany
[4]Indian Institute of Science Education and Research Mohali (IISERM), India.
[5]Earth System Division, National Institute for Environmental Studies (NIES), Japan
[6]Atmospheric Science Division, Aryabhatta Research Institute of Observational Sciences, Nainital, India

Correspondence: Dhanyalekshmi Pillai (dhanya@iiserb.ac.in)

Abstract. Devising effective national-level climate action plans needs a more detailed understanding of the regional distribution of sources and sinks of greenhouse gases. Due to insufficient observations and modelling capabilities, India's current carbon source-sink estimates are uncertain. This study uses a high-resolution Lagrangian transport model to examine the potential of available CO_2 observations over India for inverse estimation of regional carbon fluxes. We use four different sites in India that vary in measurement technique, frequency and spatial representation. These observations exhibit substantial seasonal (7.5 to 9.2 ppm) and intra-seasonal (2 to 12 ppm) variability. Our modelling framework, a high-resolution Weather Research and Forecasting Model combined with Stochastic Time Inverted Lagrangian Transport (WRF-STILT) model, performs better in simulating seasonal (R^2 = 0.50 to 0.96) and diurnal (R^2 = 0.96) variability (for Mohali station) of observed CO_2 than the current generation global models (CarboScope, CarbonTracker and ECMWF-EGG4). The seasonal CO_2 concentration variability in Mohali, associated with crop residue burning, is largely underestimated by the models. WRF-STILT captures the seasonal biospheric variability over Nainital better than the global models but underestimates the strength of the CO_2 uptake by crops. The choice of emission inventory in the modelling framework alone leads to significant biases in simulations (5 to 10 ppm), endorsing the need for accounting emission fluxes, especially for non-background sites. Our study highlights the possibility of using the CO_2 observations from these Indian stations for deducing carbon flux information at regional (Nainital) and sub-urban to urban (Mohali, Shadnagar and Nagpur) scales with the help of a high-resolution model. On accounting for observed variability of CO_2, the global carbon data assimilation system can benefit from the measurements from the Indian subcontinent.

1 Introduction

The global terrestrial ecosystem acts as a significant carbon sink. A decrease in sink capacities accelerates global warming as a consequence of the increased atmospheric emission fraction (airborne fraction). How the terrestrial carbon sink capacity responds to the rate of atmospheric greenhouse gas increase remains uncertain, implying large uncertainties in future climate

predictions. Further, significant uncertainties exist in our estimations of the magnitude and spatial distribution of carbon fluxes between land, atmosphere, and oceans (Friedlingstein et al., 2022). These estimates are particularly critical to devising effective mitigation plans for climate change. The carbon budget estimation system must sufficiently represent the complex exchange

25   processes operating at different spatial and temporal scales to address the above key shortcoming.

India needs an accurate estimation of its carbon sources and sinks to achieve its Nationally Determined Contribution (NDC) goals (https://unfccc.int, last access: 25 March 2023) through emission reduction. The bottom-up approach is widely used to estimate carbon fluxes based on our prior knowledge of the processes determining the fluxes, such as vegetation, land types, and fossil fuel usage statistics. However, these estimates are often characterised by large errors due to various factors, in-

30   cluding the reliability of statistical reports, the accuracy of flux estimation approaches, and desired spatiotemporal resolution. An inverse modelling framework ~~(top-down approach, Enting (2002))~~ (top-down approach, Enting, 2002) encompassing atmospheric transport models and observations of atmospheric carbon concentrations have the potential to improve bottom-up based estimates of the source-sink distribution of carbon globally (e.g., Rödenbeck et al., 2003; Peters et al., 2007; Inness et al., 2019) and on regional scales (e.g., Gerbig et al., 2009; Broquet et al., 2013; Pillai et al., 2016). There have been a few recent

35   inverse-based attempts to estimate the carbon fluxes over the South Asian region using in-situ and satellite observations (e.g., Patra et al., 2013; Thompson et al., 2016; Ganesan et al., 2017; Philip et al., 2022; Sijikumar et al., 2023); however, these studies are limited by the general paucity of observational data with sufficient temporal and spatial coverage over the region.

In-situ observations are essential for the tropics because satellite observations representing the entire atmospheric column cannot always detect signatures from small-scale surface flux variations. Moreover, one may expect significant data gaps in

40   satellite measurements, depending on the season, due to clouds and moist convection. Recently, more greenhouse ~~gases~~ gas (GHG) monitoring stations have been set up over India by different research initiatives (e.g., Tiwari et al., 2014; Lin et al., 2015; Mahesh et al., 2015; Chandra et al., 2016; Jain et al., 2021; Nomura et al., 2021; Sijikumar et al., 2023). High-frequency observations with diurnal and synoptic variations provide information on the regional sources and sinks for atmospheric CO_2, which are influenced by mesoscale atmospheric transport (Law et al., 2002; Gerbig et al., 2003; Geels et al., 2004; Lin et al.,

45   2004; Lauvaux et al., 2008). CO_2 anomalies generated remotely can also affect these observation sites through horizontal advection. Law et al. (2002) has suggested that the use of high-frequency observation can aid in reducing the uncertainty in inverse estimates, similar to using a larger observation network with low-frequency observations. However, measurements obtained from an observation site close to a variable source or meteorologically complex areas are difficult to represent in the transport models used for inversions. These factors must be considered while developing observation sites that can be used for

50   inverse optimisation. Due to the unavailability of long-term consistent observations representing the regional fluxes, none of the current generation global carbon assimilation systems utilises CO_2 observations from the Indian region. Additionally, to utilise the potential of these observations through inverse modelling, we need to improve our understanding of the processes driving high-frequency variability in these measurements (Geels et al., 2004). That is, sufficient improvement in modelling capabilities is required over the Indian region.

55   The skill of the model is determined by how well it can simulate the variability in atmospheric CO_2 concentration. The model-observation mismatch in atmospheric CO_2 concentrations emerges due to the combined effect of uncertainties in the

transport processes and the improper representation of CO_2 flux variability. The accurate representation of the planetary boundary layer (PBL) height is also crucial for the simulation of tracer distribution in the boundary layer and its dynamics (e.g., Gerbig et al., 2008). Most current generation carbon flux estimations over India are derived from global carbon esti-

60 mates, which utilise coarse-resolution transport models (e.g., Rödenbeck et al., 2003; Peters et al., 2007; Inness et al., 2019) for their simulations. However, atmospheric CO_2 exhibits strong spatiotemporal variations such that the transport models need a horizontal resolution higher than 30 km to represent the variability (Gerbig et al., 2003). Similarly, local and large-scale convections play a major role in distributing atmospheric tracer concentrations (Gerbig et al., 2003) vertically, which is difficult to simulate in tropical regions (Thompson et al., 2014). Fine-scale features are better resolved when the horizontal resolution

65 of transport models is increased (Geels et al., 2007; Tolk et al., 2008; Agustí-Panareda et al., 2019). Thilakan et al. (2022) showed that considerable representation errors exist when we use coarse-resolution transport models for inverse optimisation over India, and the representation error tends to decrease when we increase the horizontal resolution. The seasonally reversing monsoon circulation pattern and complex topography complicate regional atmospheric transport, influencing the vegetation patterns and agricultural practices over the region. Hence, an adequate representation of the atmospheric CO_2 distribution over

70 India relies on a modelling system that can operate at a high spatial and temporal resolution and has the ability to simulate all the essential underlying processes. There are increasing efforts in recent years to constrain the regional CO_2 fluxes over India via inverse modelling frameworks (Halder et al., 2022; Philip et al., 2022; Sijikumar et al., 2023). However, when assimilating regional measurements in the inverse optimisation framework, it is crucial to investigate how effectively the forward modelling system reproduces the observed variations associated with fine-scale transport and local influences at various time scales. This

75 is because considerable model-data mismatches due to transport errors can lead to large uncertainties in the estimated fluxes.

This study focuses on assessing the potential of four available observations over India to be employed in future high-resolution Inverse modelling frameworks to optimise regional CO_2 fluxes. We analyse the variability and representativeness of CO_2 observations from each station. Observations with high variability, often due to the influence of local flux variations, may not be suitable for regional flux optimisations but can provide important information about local emission sources. Further, we

80 examine the capability of a high-resolution modelling framework based on the Lagrangian particle dispersion model (LPDM) to simulate CO_2 variability over these observation sites. We follow the receptor-oriented framework described in Gerbig et al. (2003) using an LPDM called the Stochastic Time-Inverted Lagrangian Transport (STILT) model (Lin et al., 2003). The CO_2 observations used in this study were taken from the near-surface using different measurement techniques at different frequencies. We assess the usability of these measurements in the inverse framework when utilising the high-resolution (e.g.,

85 WRF-STILT) modelling system to optimise carbon fluxes. We quantify the model uncertainties and compare them with some of the existing coarse-resolution models.

This paper is organised as follows: Sect. 2 briefly describes the modelling framework employed in this study. In Sect 3, we provide the details of CO_2 measurements and global reanalysis data used in this study. Sect. 4 deals with the methods used for assessing the model skill in capturing observed variability. Sect. 5 presents the observed CO_2 variability across India,

90 investigating how well STILT and global models could capture these variations. In Sect. 6, we further discuss the potential of

using these observations in the future inverse modelling system, taking into account the current limitations of our modelling system. The conclusions are presented in Sect. 7.

2 Modelling framework

A receptor-oriented analysis framework was designed to quantify the sensitivity of the atmospheric CO_2 concentrations (influ-
95 ence functions) at measurement locations (receptors) to the surface fluxes in the upwind regions or boundary conditions and thereby interpret the atmospheric signatures of the surface processes. These influence functions (footprints) can be considered equivalent to the adjoint of the Eulerian transport model. This STILT modelling framework utilises meteorology from an Eulerian transport model, surface fluxes from biospheric models or inventories, and boundary conditions from global reanalysis products to simulate the atmospheric CO_2 concentration at receptor locations. The boundary conditions are intended to provide
100 the background and influence of remote fluxes on the observations. In this study, the Weather Research and Forecasting model (WRF) is used to simulate meteorology at a horizontal resolution of 10 km $\times$ 10 km and a temporal resolution of one hour. Using STILT has the advantage of simulating CO_2 variability down to spatial scales that are slightly smaller than the grid size of the meteorological fields used (Lin et al., 2003; Gerbig et al., 2003). Because it employs a backward time simulation strategy, it is more computationally cost-effective than an alternative forward time simulation (Lin et al., 2003), at least for
105 data-sparse situations with only a few observational sites.

We simulated CO_2 concentrations at the measurement locations using the WRF-STILT modelling framework. A detailed description of the WRF-STILT system can be obtained from Nehrkorn et al. (2010). The STILT is a widely used LPDM to determine the influence of surface emissions at a receptor location by simulating the transport in the near field (i.e. the surface that ~~planetary boundary layer (PBL)~~ PBL air has come into contact with before arriving at the measurement location) (e.g., Lin
110 et al., 2003; Gerbig et al., 2003; Nehrkorn et al., 2010; Pillai et al., 2011; Maier et al., 2022). The STILT model utilises the mean advection scheme used by the ~~HYSPLIT~~ Hybrid Single-Particle Lagrangian Integrated Trajectory (HYSPLIT) model (Stein et al., 2015). The turbulent motions are modelled as a Markov chain process (Lin et al., 2003). The mean wind is represented by interpolating the wind fields from numerical weather prediction models or reanalysis data (from the WRF model in this study) into the sub-grid location of the particle. STILT simulates the transport by following the backwards-in-time evolution
115 of an ensemble of particles (representing air parcels of equal mass) from receptor locations using mean winds and turbulent motions. The most critical meteorological variables required for trajectory calculations are vertical profiles of horizontal and vertical wind components (Nehrkorn et al., 2010).

In the STILT model, changes in the atmospheric CO_2 concentration, $\Delta C(\mathbf{x}_r, t_r)$ at the observation site at $\mathbf{x}_r$ and time t_r can be derived as follows:

$$
120 \quad \Delta C(\mathbf{x}_r, t_r) = \int_{t_0}^{t_r} dt \int_V dx\, dy\, dz\, I\,(\mathbf{x}_r, t_r | \mathbf{x}, t) S(\mathbf{x}, t) \tag{1}
$$

where $S(\mathbf{x},t)$ is a volume source-sink in units of $ppm\ h^{-1}$ and $I\left(\mathbf{x}_r,t_r|\mathbf{x},t\right)$ is the influence function for the receptor location which quantitatively links sources/sinks to concentrations and has a unit of m^{-3}. The quantification of the time volume integration of the influence function is achieved by counting the total length of time $\Delta t_{p,m,i,j,k}$ that each released particle p spends in a volume element (i,j,k) during a time step m and normalising to the number of particles released N_{tot} (Lin et al., 2003).

$$\int\limits_{t_m}^{t_m+\tau}\int\limits_{x_i}^{x_i+\Delta x}dx\int\limits_{y_j}^{y_j+\Delta y}dy\int\limits_{z_k}^{z_k+\Delta z}dz\,I\left(\mathbf{x}_r,t_r|\mathbf{x},t\right)=\frac{1}{N_{tot}}\sum_{p=1}^{N_{tot}}\Delta t_{p,m,i,j,k} \tag{2}$$

The link between surface fluxes $F(x,y,t)$ (in units of $mol\ m^{-2}s^{-1}$) and a volume source-sink $S(\mathbf{x},t)$ is established by diluting the surface tracer flux into an atmospheric column of height h, in the assumption that the turbulent mixing below this height is strong enough to thoroughly mix the surface flux from ground to h within one model time step m. Here, h is set to half of the PBL height, and the PBL height is calculated internally by STILT using meteorological inputs provided by WRF. These WRF meteorological simulations (temperature, moisture and wind) are compared reasonably well ($R^2 > 0.75$) with observations (Mathew et al., 2024). STILT compute the PBL height with the help of a modified Richardson number as described in Vogelezang and Holtslag (1996). The relation between $F(x,y,t)$ and $S(\mathbf{x},t)$ is summarised in Eq. (3) as follows:

$$S(\mathbf{x},t)=\begin{cases}\frac{m_{air}}{h\overline{\rho}(x,y,t)}F(x,y,t) & for\ z\leq h\\0 & for\ z>h\end{cases} \tag{3}$$

where m_{air} is the molar mass of air and $\overline{\rho}(x,y,t)$ is the average air density. From the above equations (Eqs. (1), (2) and (3)), the contribution of emission fluxes from each surface grid cell (i,j) and time step m to the total CO_2 enhancement $\Delta C(\mathbf{x}_r,t_r)$ at receptor location can be obtained as:

$$\Delta C_{m,i,j}(\mathbf{x}_r,t_r)=\frac{m_{air}}{h\overline{\rho}(x_i,y_i,t_m)}\frac{1}{N_{tot}}\sum_{p=1}^{N_{tot}}\Delta t_{p,m,i,j,k}F(x_i,y_i,t_m)=f(\mathbf{x}_r,t_r|x_i,y_i,t_m)F(x_i,y_i,t_m) \tag{4}$$

Here, $f(\mathbf{x}_r,t_r|x_i,y_i,t_m)$ is known as the "footprint" which links the CO_2 surface fluxes to CO_2 concentration changes at the observation site as mentioned before. The total CO_2 concentration enhancement $\Delta C(\mathbf{x}_r,t_r)$ at the observation site is obtained by summing $\Delta C_{m,i,j}(\mathbf{x}_r,t_r)$ over all the grid cells (i,j) and time (m).

We released 100 particles from every receptor location to calculate the back trajectories with a maximum backward time of 120 h. This period is set by estimating the approximate time required for all particles to exit the model domain. We used the time-averaged, mass-coupled velocity fields from the WRF model to avoid mass violation in STILT. The initial and boundary conditions for WRF are obtained from the ERA5 reanalysis dataset of the European Centre for Medium-Range Weather Forecasts (ECMWF). The WRF simulations over the domain are generated for 2017. The detailed description of the WRF model set up over the Indian domain used for this study can be obtained from Thilakan et al. (2022). The evaluation of the WRF

model simulations over India shows a good agreement with observations (e.g., Hariprasad et al., 2014; Boadh et al., 2016; Sivan et al., 2021; Mathew et al., 2024). ~~Mathew et al. (2024) demonstrated that temperature, moisture and wind simulations by WRF had a good correlation ($R^2 > 0.75$) in comparison with observations.~~ The footprints were calculated based on Eq. (4), which were dynamically gridded to a maximum resolution of 10 km × 10 km.

The biosphere flux distribution over the domain was generated using a biospheric model called the Vegetation Photosynthesis and Respiration (VPRM) model (Mahadevan et al., 2008). The VPRM model calculates Gross Ecosystem Exchange (GEE) and ecosystem respiration (R_{eco}) using WRF meteorological fields and MODIS (Moderate Resolution Imaging Spectroradiometer) data from Terra and Aqua satellites. Biospheric fluxes are generated at horizontal resolution 10 km × 10 km over the domain. These fluxes were utilised to calculate the atmospheric CO_2 contribution by the biosphere over the receptor locations (termed as $CO_{2_{bio}}$). Anthropogenic CO_2 fluxes were prescribed from three different inventories to represent anthropogenic contribution and also to examine the impact of emission differences in CO_2 simulations over the Indian domain. Anthropogenic emission fluxes from Emissions Database for Global Atmospheric Research (EDGAR), Open-source Data Inventory for Anthropogenic CO_2 (ODIAC) and Integrated Carbon Observation System - Global anthropogenic CO_2 emissions (hereafter referred to as ICOS) were used in this study. The EDGAR inventory (v7.0; Crippa et al., 2018, 2022) provides anthropogenic fluxes at a horizontal resolution of 0.1°×0.1°for every year. ODIAC (v2020; Oda and Maksyutov, 2020; Oda et al., 2018) has a higher spatial resolution of 1 km × 1 km but is available only at a monthly timescale. ICOS (v2019; Karstens et al., 2019; Janssens-Maenhout et al., 2019) is developed based on EDGAR v4.3 and British Petroleum statistics with a horizontal resolution of 0.5°×0.5°and a temporal resolution of hourly. All these data sets were interpolated into model resolution, conserving mass. The model included the effect of global CO_2 variability over the domain from boundary conditions (also known as background signal, $CO_{2_{bck}}$) and was added to the local CO_2 mole fraction (resulting from local fluxes) within the model domain to compare with the observations. In this study, we have used two different global reanalysis products separately as boundary conditions to understand the influence of boundary conditions on total CO_2 mole fraction. We used Jena CarboScope (version: s10c_v2020; Rödenbeck et al., 2003) and ECMWF-Copernicus Atmosphere Monitoring Service (CAMS, Version: EGG4; Agustí-Panareda et al., 2023) as boundary conditions for this study (see Sect. 3.2). We do not include the contribution from oceanic fluxes, as its influence on these stations is very negligible ($\sim$ 0.001 ppm, Figure not shown). We incorporate the influence of biomass burning separately over Mohali during the biomass burning emission season (see Sect. 6.1 for a detailed discussion).

That is, the total atmospheric CO_2 concentration (atmospheric $CO_{2,tot}$) was calculated by adding the background ($CO_{2,bck}$), biospheric ($CO_{2,bio}$) and anthropogenic ($CO_{2,ant}$) terms together to compare with the observations. The atmospheric CO_2 concentration at the measurement location is given by:

$$CO_{2_{tot}} = CO_{2_{bck}} + CO_{2_{bio}} + CO_{2_{ant}} \tag{5}$$

Atmospheric CO_2 mixing ratios at the measurement locations were retrieved at a temporal resolution of three hours. Since we used two different boundary conditions and three different anthropogenic fluxes for the WRF-STILT simulations, we have a set of six simulations (see Table 1) over each observation site. WRF-STILT simulations are hereafter referred to as simply STILT simulations in this article. The simulations with CarboScope (CS) as background are represented as STILT-CS-EDG

Table 1. A brief description of different WRF-STILT simulations and their input fluxes used in the study

No	Name of the simulation	Biospheric fluxes	Background fluxes	Anthropogenic fluxes
1	STILT-CS-EDG	VPRM	CarboScope	EDGAR
2	STILT-CS-ICOS	VPRM	CarboScope	ICOS
3	STILT-CS-ODI	VPRM	CarboScope	ODIAC
4	STILT-EGG4-EDG	VPRM	EGG4	EDGAR
5	STILT-EGG4-ICOS	VPRM	EGG4	ICOS
6	STILT-EGG4-ODI	VPRM	EGG4	ODIAC

(EDGAR as anthropogenic flux), STILT-CS-ICOS (ICOS as anthropogenic flux) and STILT-CS-ODI (ODIAC as anthropogenic flux) in this manuscript. Similarly, simulations with CAMS EGG4 (EGG4) as background are represented as STILT-EGG4-EDG (EDGAR as anthropogenic flux), STILT-EGG4-ICOS (ICOS as anthropogenic flux) and STILT-EGG4-ODI (ODIAC as anthropogenic flux).

3   Data

3.1   CO$_2$ observations over India

We used atmospheric CO$_2$ observations for 2017 from four measurement sites located at Mohali, Nainital, Shadnagar and Nagpur (see Fig. 1) to assess their temporal variability. The sites were chosen based on the availability of their long-term measurements to the research team. Also, we examine how well the STILT simulations capture these variations.

We used continuous hourly measurements of CO$_2$ using the PICARRO CRDS (Cavity Ring-Down Spectroscopy) instrument at the Mohali station. Atmospheric CO$_2$ mole fractions are measured at 20 m height above ground level. The measured CO$_2$ mixing ratios have an overall uncertainty calculated based on the root mean square propagation of individual uncertainties, such as the accuracy error of gas standard (2%), 2σ instrumental precision error (0.1% for CO$_2$), and flow reproducibility (2%), resulting in a measurement uncertainty less than 4%. The limit of detection for CO$_2$ is reported to be better than 0.5 ppm (Chandra et al., 2017). Mohali station is situated in a suburban area (30.67° N, 76.73° E; 310 m a.s.l) in the northwestern part of the Indo-Gangetic plain (IGP), close to Chandigarh city (Sinha et al., 2014; Pawar et al., 2015). The instrument facility is housed inside the campus of the IISER Mohali. More details about the measurement techniques employed for Mohali observations are available from Chandra et al. (2017). Mohali has the proximity of three cities (Chandigarh, Mohali and Panchkula), with more than 100,000 population at a distance of a few kilometres in the northeast direction, among which Chandigarh has nearly one million population. STILT footprints show that the predominant wind direction towards the observation site is northwest, except during the monsoon season, in which the wind comes in the southeast direction (Fig. S1). The northwest region of Mohali is dominated by agricultural and other rural land use patterns (Kumar and Sinha, 2021). Agricultural emission activities like

residue burning can be expected in this region during April-May and October-November period (Sinha et al., 2014). Local
influences on the measurements from the residents of IISER Mohali are expected to be minimal since the measurement facility
is located in the upwind direction of the potentially local sources inside the campus.

Weekly flask measurements of atmospheric CO_2 mole fractions from the Nainital observation site are used here (Terao et al.,
2022). Nainital observation site is located at the Aryabhatta Research Institute of Observational Sciences (ARIES) (29.36° N,
79.46° E; 1940 m a.s.l, Nomura et al. (2021)). Since the measurement location is near the Himalayan mountain range, Nainital
is considered as a background site representing north Indian GHG distribution with some influence from anthropogenic ac-
tivities, including biomass burning during spring and autumn months when air mass stays for a longer duration over northern
India (Sarangi et al., 2014; Nomura et al., 2021). The inlets for the air samples are mounted at a height of 7 m above ground
level. Weekly flask samples were collected at 14:00 local time and transported to the Center for Global Environmental Re-
search (CGER) laboratory, National Institute for Environmental Studies (NIES), Japan, for gas analyses. CO_2 analyses were
done using a non-dispersive infrared analyzer (NDIR; LI-COR, LI-6252) with an analytical precision of 0.03 ppm against the
NIES09 scale and the NIES09 and NOAA scales have a difference ranging from 0.04 to 0.09. More details are available at
Nomura et al. (2021). Near-field contributions of the Nainital station are mainly from the northwestern region of the station
except during the summer monsoon (JJA) period (Fig. S2). During the winter period (DJF), the influence region covers the
southeast of the site as well.

The observation site Shadnagar is at the National Remote Sensing Sensing Center (NRSC), Shadnagar (17.09° N, 78.21° E;
648m a.s.l). Shadnagar is a suburban station situated about 65 km from Hyderabad (Mahesh et al., 2015; Sreenivas et al.,
2016). Measurements are carried out using Los Gatos Research's Greenhouse Gas Analyser (model: LGR-GGA-24EP) at an
interval of 1 s with precision and accuracy of 0.078 ppm and 0.101 ppm respectively (Mahesh et al., 2015; Sreenivas et al.,
2016). The LGR-GGA instrument uses enhanced off-axis integrated cavity output spectroscopy (OA-ICOS) technology. A
downward-facing inlet is mounted 10 m above ground level to provide ambient airflow to the instrument. Mahesh et al. (2015)
provides a detailed description of the instrument and the calibration procedure. This study uses the daily average values of
these observations available from https://bhuvan-app3.nrsc.gov.in/data/download/index.php (last access: 12 December 2022).
The near-field influence regions of Shadnagar vary with seasons (Fig. S3). The influence region covers the northeast of the site
during post-monsoon (SON) and winter (DJF) seasons. The dominant influence on the Shadnagar comes from the west during
the summer monsoon period (JJA) and from the southeast during the pre-monsoon season (MAM).

We have also used continuous atmospheric CO_2 measurements from Nagpur installed at NRSC, Regional Centre office
(21.15° N, 79.15° E; 312 m a.s.l). Nagpur is located 7 km west of Nagpur city centre, one of the largest cities in central India,
with a population of around 2.5 million. The site's region (Deccan plateau of the Indian peninsula) includes large industries and
coal-powered power plants (Kompalli et al., 2014; Shaeb et al., 2020). Based on our STILT footprints, the major influence on the
CO_2 variability at Nagpur comes from the west (summer, JJA), northeast (post-monsoon, SON), and north-west (pre-monsoon,
MAM) of the observatory (Fig. S4). Nagpur utilises a high-precision non-dispersive infrared gas analyzer (LICOR LI-7500)
instrument mounted at 8 m height from ground level to measure the atmospheric CO_2 concentrations. Daily average values
of these measurements, available from https://bhuvan-app3.nrsc.gov.in/data/download/index.php, (last access: 12 December
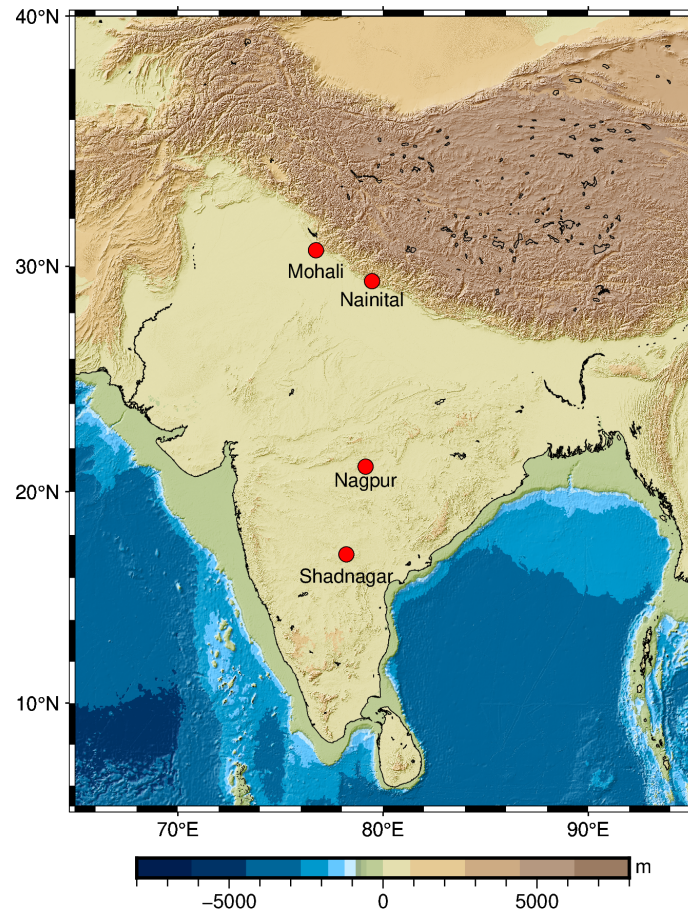
Figure 1. Location of CO_2 observation sites used in the study

2022), are used in this study. Shadnagar and Nagpur observations are carried out as part of the Climate and Atmospheric
240   Processes of the ISRO-Geosphere Biosphere Programme (CAP-IGBP).

3.2   Global Reanalysis products

We also compared CO_2 observations with three global reanalysis products to examine the model-data mismatches at these
stations. These products are ~~optimized~~ optimised with available observations of CO_2 (e.g. data from surface monitoring stations,
total column retrievals from satellites, aircraft missions, ship cruises, and AirCore balloon sounding) from different parts of
245   the world. None of these products utilises in-situ observations from India. We used atmospheric CO_2 concentration from
CarbonTracker (CT2019B; Jacobson et al., 2020), CarboScope (s10c_v2020; Rödenbeck et al., 2003; CarboScope, 2020)
and ECMWF CAMS (EGG4; Agustí-Panareda et al., 2023; Copernicus Atmosphere Monitoring Service, 2021) to compare
with the observations. All of these reanalysis products differ in their spatial and temporal resolutions. CarbonTracker has a

horizontal resolution of $3° \times 2°$ and a temporal resolution of 3 hours with 25 vertical levels. CarboScope is a comparatively

250 coarser model with a horizontal resolution of $5° \times 3.8°$ and a temporal resolution of 6 hours with 19 vertical levels. Among these products, CAMS EGG4 has the finest spatial resolution with $0.75° \times 0.75°$ in the horizontal direction with 25 vertical levels and a temporal resolution of 3 hours. To compare with the observations, simulations from the first vertical level of the CarbonTracker are used. Model simulations at 1000 mb pressure level from CarboScope and EGG4 are used to compare the observations at Mohali, Shadnagar and Nagpur. Since Nainital is a mountain site situated at $\sim$ 800 mb height, we compared

255 those observations with CarboScope and EGG4 products at 800 mb vertical level.

4   Assessment of modelling skill

We have derived different statistical indices to examine the performance of the model simulations to predict the CO_2 variability. To quantify the error distribution between model (P) and the observation (O), we have calculated the Root Mean Square Error (RMSE) and the Mean Absolute Error (MAE) between the model simulations and observations.

260   To separate the systematic and unsystematic components from the RMSE, we have used the following method proposed by Willmott (1981). Systematic RMSE is obtained as:

$$RMSE_s = \sqrt{\frac{1}{n}\sum_{i=1}^{n}(\hat{P}_i - O_i)^2} \tag{6}$$

and the unsystematic RMSE as:

$$RMSE_u = \sqrt{\frac{1}{n}\sum_{i=1}^{n}(P_i - \hat{P}_i)^2} \tag{7}$$

265 where $\hat{P}_i = a + bO_i$

Here a and b respectively are the intercept and slope of the least squares regression. The systematic difference for a 'perfect' model is expected to be very close to zero, while the unsystematic difference remains close to the value of RMSE. Based on Willmott et al. (2012), we have also computed the refined index of agreement (d_r) as follows:

$$d_r = \begin{cases} 1 - \dfrac{\sum_{i=1}^{n}|P_i - O_i|}{c\sum_{i=1}^{n}|O_i - \overline{O}|}, & \text{when } \sum_{i=1}^{n}|P_i - O_i| \le c\sum_{i=1}^{n}|O_i - \overline{O}| \\ \dfrac{c\sum_{i=1}^{n}|O_i - \overline{O}|}{\sum_{i=1}^{n}|P_i - O_i|} - 1, & \text{when } \sum_{i=1}^{n}|P_i - O_i| > c\sum_{i=1}^{n}|O_i - \overline{O}| \end{cases} \tag{8}$$

270   Here, the constant c is set to 2 (Willmott et al., 2012). The d_r values can range from -1 to 1. It indicates the sum of error magnitudes between predicted and observed values relative to the sum of observed deviations around the observed mean. For

example, $d_r = 0.5$ indicates that the sum of the model-observation mismatch is half the sum of the observed variability around the mean. i.e. d_r gives a relative magnitude of the model error compared to the variance of the observations.

5 Results

275 ### 5.1 Observed CO_2 variability over India

To assess the CO_2 variability over India during 2017, we analysed in-situ observations of atmospheric CO_2 from four different sites (see ~~See~~Sect. 3.1).

Mohali observations show strong variability due to its proximity to urban areas (see Fig. 2a). Mohali has hourly observations, and we have separated the daytime values (11:00-16:00 Local time) to distinguish the influence of the nocturnal boundary layer

280 on observations (see Fig. 2a). The annual mean of hourly atmospheric CO_2 concentration at Mohali (whole day) during 2017 is 428.8 ppm with a standard deviation (σ) of 26.6 ppm. For the daytime, the annual mean CO_2 is approximately 20 ppm less (408.3 ppm) than all-time, with a variability (σ) of 11.6 ppm. Since most of the inverse models, which target to retrieve surface-atmosphere exchange fluxes from in-situ observations, use daytime measurements, we carry out the rest of our analysis for Mohali based on daytime values (unless specified otherwise). Monthly mean values of daytime observations show that Mohali

285 exhibits strong seasonal variability (σ = 9.2 ppm) with approximately a 32.9 ppm difference between maximum and minimum values (see Fig. S7). Maximum intra-month variability is found during January, September, November and December, with a standard variability of 8-12 ppm (Fig. 2a). On a monthly scale, lower values are seen during February (397.9 ppm) and August (391.2 ppm) and higher values during May (413.5 ppm) and November (424 ppm) (Fig. 3a). As expected, the atmospheric CO_2 concentration decreases from June onwards due to the enhanced biospheric activity associated with summer monsoon rainfall

290 (Fig. 3a). However, we find high CO_2 concentrations at Mohali during November, which can be attributed to the agricultural waste-burning activities prominent around this region at this time of the year (Deshpande et al., 2023). A detailed discussion on the influence of biomass burning on CO_2 concentration over Mohali is provided in ~~See~~ Sect. 6.1. In general, measured CO_2 concentration over Mohali shows considerable influences from local fluxes (see Fig. S5).

Mohali observations show strong diurnal variability (σ = 14.7 ppm) as well with up to 40 ppm difference between the

295 maximum and minimum concentrations during the early morning (06:00 LT) and the afternoon (15:00 LT), respectively (Fig. S6). Due to strong mixing, variability in CO_2 concentration is less ($\sigma \approx$ 12 ppm) during daytime (12:00-15:00 LT) compared to the nocturnal variability of 19-32 ppm (see Fig. S6). A similar reduction in CO_2 variability can be seen at 09:00 LT during May-August (Fig. S7), most likely due to a well-established convective boundary layer with strong mixing. Nocturnal CO_2 variability during March-May is less compared to other seasons. Apart from this, Mohali observations do not show considerable

300 differences in their diurnal cycle among seasons (Fig. S7).

Monthly mean observations from Nainital also show strong seasonal variations (σ = 7.5 ppm) in CO_2 concentrations (Fig. 3c) with a difference of up to 25 ppm, between the maximum (412.8 ppm) and minimum (387.9 ppm) concentrations during April and September respectively. Nomura et al. (2021) also reported a similar seasonal cycle over Nainital, with lower values during February-March and September. The observations show an annual mean of 401.6 ppm with a variability reaching 8.4

Figure 2. CO$_2$ monthly variations over different stations during 2017. Observed CO$_2$ variability is shown in comparison with STILT simulations and global reanalysis products. Box and whisker plot of observation in comparison with model simulations is shown. The box denotes the interquartile range, and the whiskers represent the points within 1.5 times the interquartile range from the lower and upper quartile. Additionally, mean values for the CO$_2$ concentration are provided as a black circle inside the box. Daytime (11:00-16:00 local time) values of the Mohali observations and simulations are used.
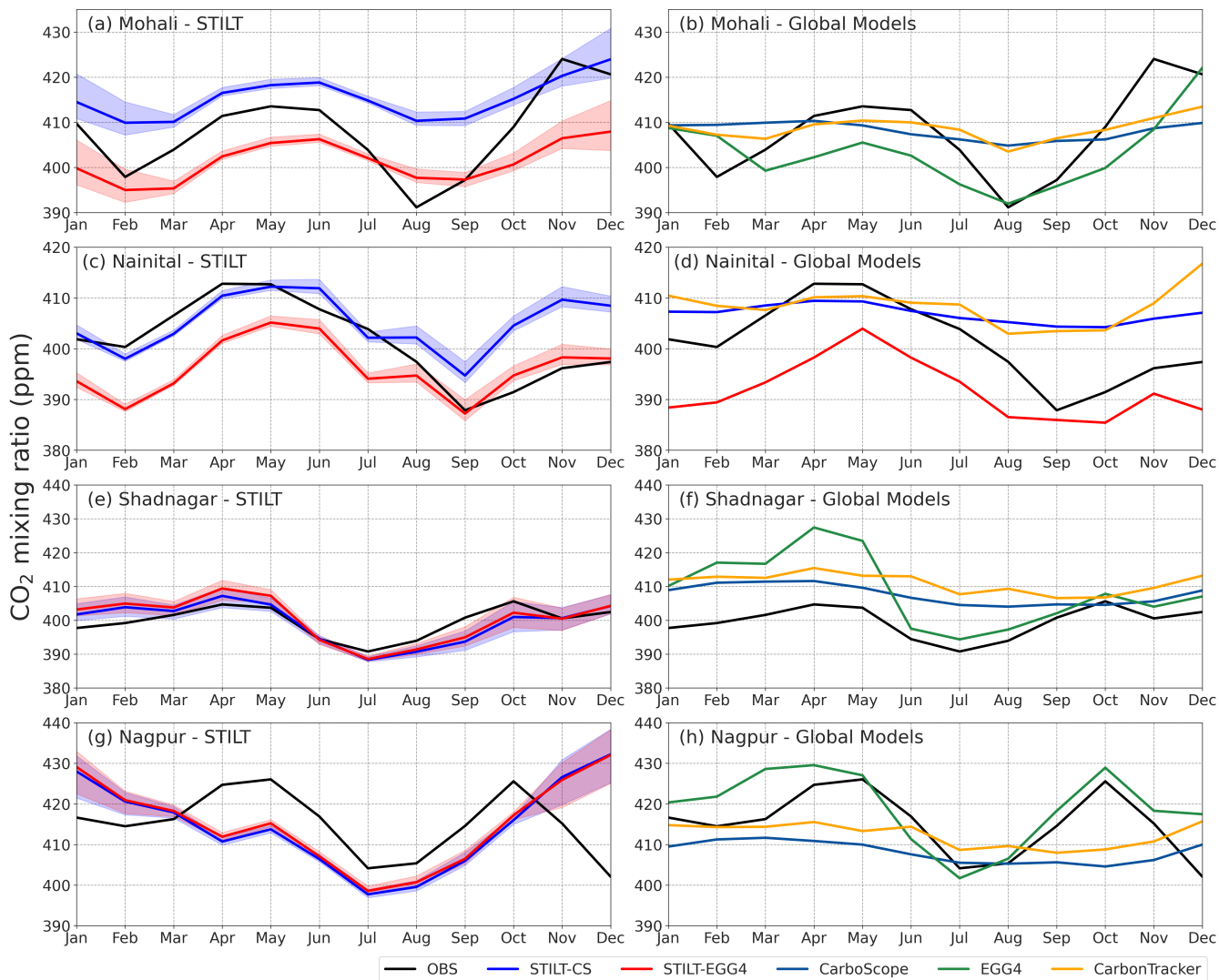
Figure 3. CO_2 seasonal cycle for different stations. Monthly mean values of CO_2 observations in comparison with STILT simulations (left panel) and global models (right panel) are given. Blue (STILT-CS) and red (STILT-EGG4) curves represent the ensemble average of the STILT simulations using different anthropogenic fluxes. Shaded regions represent the range of the model simulations.

ppm during 2017. Considerable intra-month variations at Nainital are observed during August, October and December with a variability of ~ 6 ppm (Fig. 2b & Fig. S8). In August, CO_2 concentrations show a sharp decrease in the concentration of ~ 18 ppm from previous values at the beginning of the month (~ 408 ppm, see Fig. 3c).

The annual mean of daily Shadnagar observations was 399.6 ppm during 2017 with a standard deviation of 6.2 ppm (Fig. 2c). At Shadnagar, measurements show a seasonal CO_2 variability of 4.4 ppm, with two higher peaks during April (404.7 ppm) and October (405.6 ppm), while Sreenivas et al. (2016) reported only one seasonal peak during pre-monsoon. The lowest

concentration is observed during July (390.8 ppm), with a difference of 14.8 ppm from the highest monthly concentration (Fig. 3e). In general, Shadnagar observations have not shown much intra-month variability ($\sigma \approx 2$ ppm, see Figs. 2c & S9) except during the period from August to October (σ ranges from 5.2 to 8.3 ppm). Only daily mean observations from Shadnagar are available for analysis, not hourly data as desired.

315   The CO_2 measurements at Nagpur during 2017 show an annual mean of 415.2 ppm, with a variability of 9.5 ppm (Fig. 2d). Nagpur observations show seasonal variability ($\sigma = 7.7$ ppm) with two maxima and one minimum value with ~ 22 ppm difference between these peaks (Fig. 3g). Enhanced CO_2 concentrations are observed during May (426.0 ppm) and October (425.6 ppm). In July, the Nagpur observations show lower concentrations (404.14 ppm) than the rest of the period. A sharp reduction of CO_2 concentration (~ 13 ppm) is found from October to December (see Fig. 3g & S10). Mostly Nagpur CO_2
320   observations indicated ~ 4 ppm variability within a month (see Figs. 2g & S10), except in June (6.4 ppm), September (9.8 ppm) and October (7.6 ppm). Here also, we only have access to daily mean observations from Nagpur, not hourly data.

5.2   Comparison between Observations and WRF-STILT model Simulations

We assessed how well the STILT model simulations agree with observed CO_2 variability. For the comparison, we used observations from all four stations described in Sect. 3.1 and a set of six STILT CO_2 simulations (see Eq. ~~5~~(5)) as described in Sect.
325   2.

Figure 2a shows the comparison of Mohali daytime observations during 2017 with the STILT simulations. Overall, STILT simulations capture the observed daytime variations reasonably well, with slight overestimation for STILT-CS simulations and slight underestimation for STILT-EGG4 simulations. Similar to observations, STILT simulations during March-July show less intra-month variability. The maximum variability is found during the winter months. A detailed discussion on the differences
330   in CO_2 simulations while using EGG4 and CarboScope as the initial and boundary conditions is provided in Sect. 6.4. STILT simulations with ICOS anthropogenic fluxes showed higher variability ($\sigma \approx 7.3$ ppm) than the other simulations.

Though STILT simulations capture the seasonal CO_2 variability in monthly averaged daytime values over Mohali (see Fig. 3a), the models failed to represent a sharp decline in CO_2 concentration during December. ~~This may be~~ The observed decline is likely due to the increased biospheric uptake by Rabi crops during this period~~(see~~, which may be misrepresented in the
335   biospheric model. This is further examined in detail in Sect. 6.5~~)~~. At the same time, monthly averaged values of daytime observations show a second dip in February, which is captured reasonably well by the STILT simulations (Fig. 3a). The simulations could reasonably reproduce the biospheric uptake in August by showing the lowest CO_2 concentration in August, similar to observations. The correlation coefficient between monthly averaged observations and STILT simulations varies between 0.86 to 0.89 (STILT-CS) and 0.76 to 0.87 (STILT-EGG4). At a monthly scale, STILT-EGG4 simulations underestimate
340   the seasonal cycle over the Mohali (RMSE: 6.7 - 10.0 ppm), while STILT-CS simulations show an overestimation (RMSE: 8.2 - 11.5 ppm). STILT simulations show an RMSE of 8-9 ppm with the observed intra-seasonal variability in Mohali. The intra-seasonal variability is derived by removing the monthly mean values from the CO_2 concentration.

The annual averaged diurnal CO_2 concentration shows a good correlation (see Fig. S6) between observation and STILT simulations (0.97-0.99). But there is a significant bias in the STILT-simulated diurnal cycle (see Fig. S6), which is higher

Figure 4. An overview of the performances of different models (see Sect. 4). Bar plots represent the different RMSE (in teal), systematic RMSE (RMSE$_s$, in lime green) and unsystematic RMSE (RMSE$_u$, in orchid) values estimated for each station. MAE (●), observed standard deviation (✕) and model standard deviation (✚) are overlied on barplots. The blue and black lines represent the index of agreement (d$_r$) and correlation coefficient (r) values, respectively. The panels represent (a) Mohali, (b) Nainital, (c) Shadnagar, and (d) Nagpur stations.

for STILT-EGG4 simulations (7.0-18.5 ppm) compared to STILT-CS simulations (5.4-8.2 ppm). The estimated bias is small during summer (MAM) compared to other seasons (Fig. S7). Observations and STILT simulations show less variability during daytime (12:00-18:00) compared to other periods and also have a good model-data agreement during daytime (Fig. S6).

Figure 4 summarises the statistical indices (see Sect. 4) estimated for assessing the model skills. At the Mohali station, STILT CO_2 daytime simulations show a standard variability (Fig. 4a) ranging from 5.3 - 7.3 ppm during 2017, lower than the observed standard variability (11.6 ppm). RMSE for STILT simulations shows a maximum of 13.6 ppm (STILT-CS-ICOS) and a minimum of 10.4 ppm (STILT-EGG4-ICOS). MAE values follow the same pattern as RMSE with reduced magnitude. STILT simulations show a reasonable correlation with observations with coefficient values ranging from 0.53 (STILT-EGG4-EDG) to 0.61 (STILT-CS-ODI). The index of agreement estimated for Mohali varies from 0.44 (STILT-CS-ICOS) to 0.66 (STILT-CS-ODI), indicating that the error values have a magnitude less than or equal to the variability of observations. Analysis of these indices for different months indicates that STILT has comparatively better prediction capability in summer (March-June) than the rest of the period (Figure not shown). The above results show the models' difficulty reproducing mixing during monsoon and winter. An inadequate representation of biospheric flux activities in the model can also result in observation-model mismatches. The model skill indices estimated for November are poor owing to the likely misrepresentation of variability associated with biomass burning during these months (Sinha et al., 2014; Pawar et al., 2015).

At Nainital, STILT simulations captured the CO_2 variability reasonably well, except in the winter period (Figs. 2b & 3c). An offset of 5 ppm is used in STILT-CS simulations at Nainital to minimize the consistent overestimation by the model (i.e. 5 ppm is subtracted from the initial $CO_{2_{bck}}$ component). A sharp reduction in observed CO_2 concentration from August (Fig. 3c) was not captured by the models (see Sect. 6.5 for a detailed discussion). Noticeably STILT-EGG4 simulations showed an underestimation of CO_2 values from January to May. The simulations have a standard deviation of ~ 6 ppm (6.2 - 7.1 ppm) in CO_2 concentration during 2017, which is lower than the observed standard deviation (Fig. 4b). The RMSE estimated for STILT simulations over Nainital varies between 7.3 to 9.0 ppm. STILT simulations show a reasonable correlation with the observations with a correlation coefficient of ~ 0.6, except for simulations using ICOS anthropogenic emission fluxes. We get an index of agreement of ~ 0.5, indicating that the magnitude of STILT model error is half that of the observed variations about the observed mean at Nainital. The estimated mismatches for intra-seasonal variability between observation and STILT simulations at Nainital is ~ 4 ppm (based on RMSE).

Comparison of CO_2 observations with the model simulations at Shadnagar shows that the STILT models can predict the seasonal cycle very well (see Figs. 2c & 3e) with an RMSE of ~ 4 ppm and correlation ranging from 0.75 to 0.87. Like Nainital, we reduced an offset of 20 ppm in STILT-CS simulations and 5 ppm in STILT-EGG4 simulations to correct the initial $CO_{2_{bck}}$ component. STILT reasonably reproduces the observed intra-month variability except from August to October (Figs. 2c & S9). For Shadnagar, the standard deviation of STILT simulations is higher than the observations (6.2 ppm) and ranges from 6.2 to 8.5 ppm. Estimated RMSE values for STILT simulations are comparatively low at Shadnagar and range from 6.2 to 7.2 ppm (Fig. 4c). MAE values vary from 4.3 to 5.5 ppm and follow a similar pattern as RMSE. STILT simulations show a reasonable correlation (0.55-0.67) with the observations at Shadnagar. But the index of agreement is close to zero for two simulations (STILT-EGG4-ODI and STILT-EGG4-ICOS), indicating a model error in the simulations as high as observational variability.

380 All STILT simulations show less model skill from August to November. STILT-EGG4 simulations show comparatively less model skill during January-May (Figure not shown). The estimated intra-seasonal variability shows an RMSE of 4.3 - 6.0 ppm with STILT simulations over Shadnagar.

STILT simulations at Nagpur capture the observed seasonal variability except for the winter season (Figs. 2d & 3g). The models represent the seasonal cycle from March to October over Nagpur with a correlation coefficient of ~ 0.97 and RMSE of
385 ~ 9 ppm. We reduced an offset of 15 ppm in STILT-CS simulations. The STILT simulations overestimate the winter variability. Also, the intra-month variability at Nagpur is overestimated during winter (Figs. 2d & S10). STILT simulations show an RMSE of 6.5 - 11.5 ppm with the estimated intra-seasonal variations over Nagpur. Notably, the observed decrease in CO_2 concentration during the summer monsoon season is well-captured by STILT (Figs. 2d & 3g). However, the increase in the CO_2 concentration in STILT simulations during winter months (November-February) is absent in CO_2 observations over Nagpur (Fig. 3g). The
390 skill indices for the Nagpur station show that the standard deviation of STILT simulations (10.1-17.9 ppm) is higher than observed standard deviations (Fig. 4d). Also, higher RMSE (10.5-17.5 ppm) are estimated for STILT simulations at Nagpur. Model simulations show very poor correlation coefficient values and index of agreement values at the Nagpur region for 2017. We obtained a better observation-model agreement when excluding winter months (November-February). Analysis of model skill indicates that the June-August period has low RMSE, which can be associated with strong mixing by monsoon winds
395 (Figures not shown).

5.3 Comparison between Observations and Global Reanalysis products

We compared observations with three global reanalysis products (CarbonTracker, CarboScope and EGG4) described in Sect. 3.2. The global reanalysis products (except EGG4) could not capture the seasonal variability in CO_2 over Mohali (Fig. 3b). The intra-month variability is less in daytime simulations of global models (Fig. 2a) except for EGG4 simulations during winter
400 months (November-February). CarbonTracker and CarboScope show much lower seasonal and intra-seasonal variability over Mohali (Fig. 3b). Global models show an RMSE of ~ 10 ppm with intra-seasonal variability of observations over Mohali. CarbonTracker exhibits diurnal CO_2 variability with a significant underestimation (Fig. S6). EGG4 captured the diurnal variability reasonably well, with a considerable nocturnal bias (Fig. S6). Note that the EGG4 has the highest spatial and temporal resolution among the global reanalysis products used in this study. Also, long-range transport has a strong influence on the Mohali
405 site (Pawar et al., 2015), which might contribute to EGG4's better performance. The inter-model differences in intra-month variability are large over Mohali (Fig. 2a), with the standard deviation ranging from 1.9 (CarboScope) to 9.8 ppm (EGG4). The RMSE for global model simulations varies from 10.2-12.0 ppm with correlation coefficients ranging from 0.36-0.52 (Fig. 4a). While we consider the index of the agreement, EGG4 show lower values (0.47) compared to other products, indicating that the magnitude of the error is approximately half of the observed variations.
410 CarboScope and CarbonTracker also did not capture the seasonal variability in CO_2 concentration at Nainital. Though it underestimated the variability, EGG4 showed good agreement with the seasonal variations in observations (see Fig. 3d). These reanalysis products show significant differences in CO_2 variability with standard deviations varying as 1.8 ppm (CarboScope), 4.4 ppm (CarbonTracker) and 6.9 ppm (EGG4). The observed standard deviation was higher than the standard deviation in

these products (Fig. 4b) except for EGG4. EGG4 has the maximum RMSE (11.4 ppm) among all products. CarbonTracker also shows a higher RMSE with 10.6 ppm than CarboScope (8.8 ppm). CarboScope and EGG4 models show high correlation values (~ 0.8) compared to CarbonTracker simulations. EGG4 has a very low index of agreement compared to other model simulations, which indicates that the error in the model simulations is very high compared to the observed variability. A model-observation mismatch of ~ 5 ppm (RMSE) is observed in the intra-seasonal variability estimated over Nainital.

The standard deviation of EGG4 (12.4 ppm) simulations is higher than the observed standard deviation at Shadnagar. But CarbonTracker and CarboScope predicted variability lower than that of the observation (Fig. 4c). EGG4 capture the seasonal cycle over Shadnagar reasonably well but shows high positive bias, reaching up to ~ 20 ppm during January-May (Fig. 3f). CarbonTracker and CarboScope could not capture the seasonal variability over Shadnagar. The intra-seasonal variability was also poorly represented (Fig. S9) by these products. EGG4 shows the highest RMSE (13.7 ppm) among the global models. The correlation of reanalysis products with Shadnagar observations is low (0.24-0.32) except for EGG4 (0.56) simulations. However, the index of agreement is less than zero for the EGG4 product, indicating the presence of noise in the simulations. Global models show an RMSE of up to 7 ppm with intra-seasonal variability of observations over Shadnagar.

Among global models, EGG4 shows better agreement with the observations at Nagpur, though the variability compared to observations is very high (Fig. 2d). The decline in CO_2 concentration during the summer monsoon season is captured by the EGG4 model (Figs. 3h & Fig. S10). EGG4 shows good agreement with the monthly averaged observations at Nagpur. But CarbonTracker and CarboScope do not capture the variability in the seasonal cycle well. The standard deviation of EGG4 (14.7 ppm) at Nagpur is higher than the observed standard deviation (Fig. 4d). However, the standard deviations of CarboScope (2.7 ppm) and CarbonTracker(3.4 ppm) are lower than the observed standard deviation. The estimated RMSE at Nagpur varied from 9.3 to 11.2 ppm. Similar to STILT simulations, global model simulations also show very poor correlation coefficient values at Nagpur for 2017. The estimated intra-seasonal variability between global models and observations over Nagpur shows an RMSE of up to 10 ppm.

6   Discussions

In the previous sections, we have seen that the STILT model has improved capabilities in simulating these fine-scale variabilities. Here, we critically examine how well our modelling system can utilise observations from India to deduce optimal information on underlying fluxes at different spatial and temporal scales. The major implications of our results are discussed here, with the interest of further improving the carbon data assimilation over India.

We begin this section by exploring the shortcomings that need to be addressed to use potential CO_2 observations from India for inverse optimization optimisation (see Sect(s) 6.1 - 6.3). This is because three of the four observation sites used in this study (Mohali, Shadnagar and Nagpur) are situated near cities and are characterised by large intra-seasonal variability. Observations from all these four sites show strong seasonal variations in CO_2 concentrations (see Sect. 5.1), contributed by biospheric flux variations and transport mechanisms. Along with the seasonal variations, these observations (except Nainital) are also characterised by strong small-scale variability associated with local flux variations and mesoscale transport processes.

It is thus challenging for coarse-resolution models to utilise them for inverse ~~optimization~~optimisation. Thus, an account of contributions from different sources to the total observed CO_2 is discussed in Sect. 6.4, providing useful information about the underlying processes that these observations may carry.

450   Typically, the highest CO_2 concentrations are observed during the April-May period and the lowest values are observed during July-September. The seasonal decrease in CO_2 concentration is associated with increased biospheric uptake owing to monsoon rainfall. The seasonal progression of the biospheric uptake across India can also be seen in the observations. That is, observations from the northern part of India (Mohali, Nainital) show the seasonal troughs in CO_2 concentrations approximately one month after the seasonal troughs in southern Indian stations (Shadnagar, Nagpur). This time lag in ecosystem uptake for

455 northern Indian sites is caused by the monsoon trajectories that result in different arrival times for precipitation across India. Interestingly, Nainital observations indicated a strong biospheric uptake during October-December, which all models (including WRF-STILT) failed to capture. The potential of using Nainital observations via high-resolution inverse modelling to improve the ecosystem uptake and release is further elucidated in Sect. 6.5.

     Using the systematic and unsystematic error components in model-data disagreements, Sect. 6.6 discusses the extent to

460 which our model can utilise the full potential of the observations over India, thereby assessing the potential of observations to increase the confidence levels of the derived fluxes.

6.1   Influence of biomass burning on CO_2 variability

Agricultural residue burning makes up the major share of biomass burning across India (e.g., Kumar et al., 2011). So, the spatiotemporal extent of biomass fires over India closely follows the area and period of crop harvest. Thus, a greater extent of

465 biomass burning is expected for pre-monsoon and post-monsoon seasons than for the monsoon season. Considerable aerosols and trace gas emissions are associated with these open agricultural residue burning in Indo Gangetic Plains (IGP) and Central India (Bhardwaj et al., 2016; Ravindra et al., 2022; Deshpande et al., 2023). For example, the CO_2 emission estimated from biomass burning over Punjab (a northern Indian State in which Mohali is located) is 15.62 $MtCO_2yr^{-1}$ for the year 2017 (Deshpande et al., 2023). Among the Indian states, Punjab has one of the highest rates of agricultural burning (Sahu et al., 2021;

470 Ravindra et al., 2022; Vellalassery et al., 2021; Deshpande et al., 2023). Consequently, we found a considerable influence of agricultural biomass burning on observations at Mohali during November 2017. Many biomass-burning activities were reported in late October and early November 2017 (https://firms.modaps.eosdis.nasa.gov, last access: 14 April 2023). Atmospheric CO_2 concentration increased up to 50 ppm, likely in response to the residue burning, with maximum concentration observed during 5-13 November 2017 (see Figs. S5 & S11b). STILT-derived footprints (Fig. S1) during November cover the northwest region

475 of Mohali, indicating the possible influence of biomass burning on the observed variability at Mohali. We find a considerable increase in the MODIS-derived fire counts (MODIS-FIRMS, 2021) for October and November 2017 over the Mohali footprint region (see Fig. S11a). A sharp increase in the number of fire occurrences during late October and early November is very likely due to agricultural waste burning after the harvest. We have conducted STILT simulations using biomass burning fluxes from Global Fire Assimilation System (GFAS) fluxes (Kaiser et al., 2012), and Fire INventory from NCAR version 2.5 (FINNv2.5)

480 fluxes (Wiedinmyer and Emmons, 2022; Wiedinmyer et al., 2023). Both of these data have a horizontal resolution of 0.1°×

0.1°and a temporal resolution of one day. The biomass emission fluxes over the footprint region of Mohali closely follow the fire count data (see Fig. S11a). GFAS emission fluxes over the Mohali footprint region are much less than FINNv2.5 (Fig. S11a). STILT simulations using FINN (STILT-FINN) indicate some influence from biomass burning with a time-lead with the CO_2 observations (see Fig. S11b). However, STILT simulations using GFAS (STILT-GFAS) could not represent the CO_2 contributions from biomass burning (Fig. S11b). The magnitude of CO_2 enhancement due to the biomass burning from STILT simulations is 3 ppm, which is $\sim$ 15 times less than the magnitude of the emission enhancement observed in the CO_2 observations (see Fig. S11b). This suggests that the emission inventories need to be improved further to accurately simulate the CO_2 variability due to biomass burning in the region. The reanalysis products also failed to capture the variability associated with biomass burning (see Fig. S5). Besides the inaccurate estimation of mixing height, misrepresentation of emission fluxes, as seen here, can lead to significant errors in the simulated distribution of CO_2. This result shows the role of high-resolution fluxes that can account for small-scale events like agricultural waste burning in representing CO_2 variability at Mohali.

6.2 Influence of emission uncertainties on CO_2 simulations

On estimating terrestrial carbon fluxes, inverse modelling systems usually assume a known contribution from anthropogenic emissions. However, this assumption would be problematic when we utilise observations near urban locations strongly influenced by anthropogenic emissions. For instance, the mean $CO_{2_{ant}}$ component at Mohali varies as much as 4 ppm between different emission inventories (EDGAR:3.1 ppm, ODIAC:2.5 ppm and ICOS:7.1 ppm, see Figure 5). Similarly, an emission contribution difference of up to 5 ppm, as shown by Shadnagar and Nagpur simulations, also has the potential to bias the inverse flux estimations (Houweling et al., 2010; Schuh et al., 2019). At the same time, Nainital shows the least differences among emission contributions (EDGAR:1.3 ppm, ODIAC: 1.3 ppm and ICOS:3.8 ppm), where the above assumption is unlikely to propagate large errors in terrestrial carbon estimations. The choice of emission inventory matters in the regional inverse systems since they may control the majority of CO_2 variability when urban sites are ~~utilized~~utilised. Our results demonstrate large differences among the $CO_{2_{ant}}$ simulations utilising different inventories, indicating the knowledge gap in the emission estimations.

6.3 Sensitivity of simulations to initial CO_2 distribution

STILT prescribes the initial concentration from global models to add the influences from the far-field fluxes to the site simulations. The spatiotemporal details in the prescribed global model can thus influence the STILT CO_2 simulations. The differences between the two global reanalysis products used in our STILT simulations caused considerable inter-model mismatches in Mohali (14 ppm) and Nainital (9 ppm) (see Fig. 5, Background) while resulting in a negligible bias in Shadnagar and Nagpur. Hence, the uncertainty in representing far-field influences may cause systematic bias in simulated CO_2 concentrations, depending on the sites.
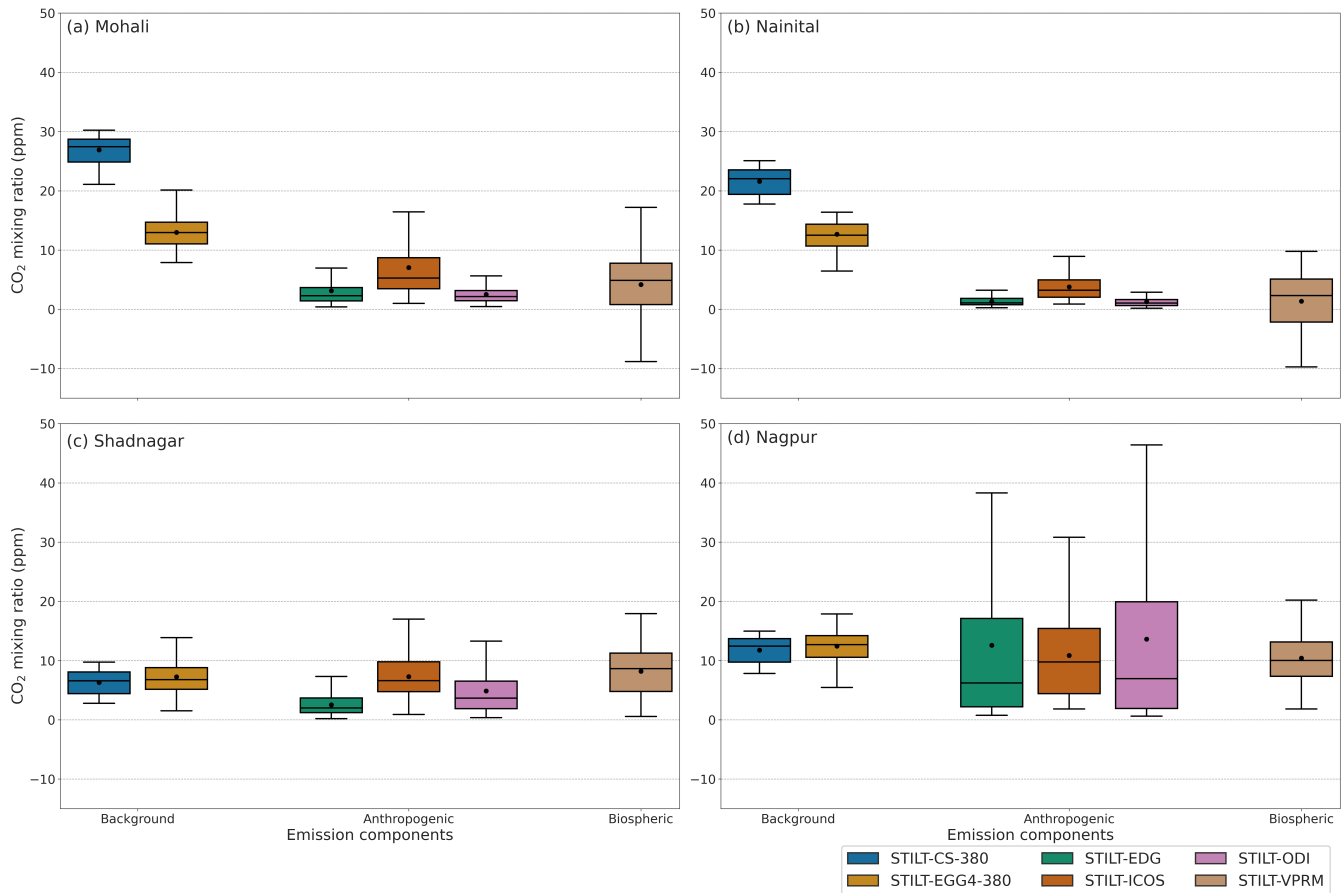
Figure 5. Variability in STILT CO_2 emission components at different stations. For better comparison with other emission components, 380 ppm is reduced from background components. The box denotes the interquartile range, and the whiskers represent the points within 1.5 times the interquartile range from the lower and upper quartile. Additionally, mean values for the CO_2 concentration are provided as a black circle inside the box. The panels represent the variability in (a) Mohali daytime (11:00-16:00 local time) simulations, (b) Nainital, (c) Shadnagar and (d) Nagpur simulations.

6.4 Relative contribution of CO_2 components to variability

Here we discuss the contribution from different components, viz. background ($CO_{2_{bck}}$), biospheric ($CO_{2_{bio}}$) and anthropogenic ($CO_{2_{ant}}$) to the total CO_2 concentration.

The CO_2 variability over an observation site is influenced by the flux variability over its footprint region (see Figs. S1-S4). In the context of the inverse modelling that optimises CO_2 flux components (such as biospheric, anthropogenic, or both), it is important to ensure considerable information gain of relevant components when observations from a particular site are utilised. So here, we investigate the relative contribution of different components to the total CO_2 concentration from each observa-

tion site. On an annual scale, observations from Mohali, Shadnagar, and Nagpur sites contain contributions from local fluxes (anthropogenic and biospheric components) by approximately six per cent of the total concentration (see Fig. 5). Regionally advected signals (background component) mostly contribute (99 % of the total) to the Nainital site. CO_{2ant} and CO_{2bio} show almost equal annual contributions in magnitude to the total CO_2 concentration in these sites. At the same time, the proportions of contributions to the total CO_2 can vary with seasons, such as winter (DJF), pre-monsoon (MAM), monsoon (JJA) and post-monsoon (SON) (Figures not shown) due to variations in atmospheric mixing and local fluxes. For instance, the reduction in CO_{2bio} component over Shadnagar and Nagpur during JJA can be very likely due to increased uptake and mixing during the monsoon period.

There are large differences in local fluxes that drive observed CO_2 variability over different sites. Mohali and Nagpur have CO_2 variability dominated by anthropogenic activities ($\sigma \approx 5.4$ to 13 ppm), while most of the CO_2 variability at the Nainital station, situated in the foothills of the Himalayas, is caused by biospheric activities ($\sigma = 5.5$ ppm)(see Fig. 5). Annually, anthropogenic and biospheric components almost equally contribute to Shadnagar variations ($\sigma \approx 2.9$ to 4.2 ppm).

6.5   Impact of biospheric uptake by crops on CO_2 variability

Biospheric fluxes determine CO_2 variability at Nainital as indicated by the STILT simulated CO_{2bio} component, which shows a similar seasonal cycle as that of the CO_2 observations (Fig. S12a). However, the simulated biospheric contribution changes from a negative (sink) to a positive (source) sign during October, while the model significantly overestimates the CO_2 concentration (Fig. 3c, Fig S12a). This overestimation corresponds to the misrepresentation of biospheric uptake of about 127 % in the influence region during October-December by the VPRM model. The improved model's correlation with observations (correlation coefficient: 0.80) and RMSE values (reduced to ~ 5 ppm) after adjusting the biospheric component (increasing 127 % of biospheric uptake during October-December in the total influence region) increases confidence in simulated transport at Nainital (Figures not shown). Thus, the above results demonstrate the potential of using Nainital observations via high-resolution inverse modelling to inform about the biospheric fluxes.

The variations in CO_{2bio} over Nainital are dominated by crop production (see CO_2-NEE_CROP in Fig S12a). The variability in the Normalized Difference Vegetation Index (NDVI, https://developers.google.com/earth-engine/datasets/catalog/COPERNICUS_S2_SR_HARMONIZED, last access: 25 June 2023) in the footprint region of Nainital, retrieved by Sentinel-2 Multispectral instrument (MSI) shows a similar pattern as of the Nainital CO_2 observations (see Figs S2 and S12b). The influence region of the Nainital site covers the Indian states Uttarakhand, Himachal Pradesh and parts of Punjab, Haryana and Uttar Pradesh. The close association of NDVI patterns with the Kharif and Rabi cropping seasons over the region confirms the enhanced ecosystem uptake due to agricultural activities (Fig. S12b). For example, NDVI increased from July, peaking at the end of August and remained high until October. The Kharif crop cultivation season usually starts in June-July, with a harvesting period from October to November. Further, NDVI increased in December, with another peak in February. Rabi cultivation typically happens around November; these crops are harvested in March-April. The lowest NDVI values for this region are associated with the harvesting period in April-May. Hence, the decrease in CO_2 concentration at Nainital during August can be very likely due to the strong uptake of Kharif crops from the upwind locations of the Nainital station. A slight

decrease of Nainital CO_2 concentration at the end of December is in response to the biospheric uptake by Rabi crops (Umezawa et al., 2016). Nomura et al. (2021) also suggests the influence of cropping patterns over IGP on Nainital observations. Noticeably, the simulated CO_2 uptake component (contribution from Gross Primary Production (GPP), see Fig. S12a) from crops shows a similar pattern as that of the Sentinel-2 derived NDVI (see Fig. S12b) in the influence region of Nainital. At the same time, the simulated CO_2 component due to the crop's respiration also shows a similar magnitude of contribution as of uptake, nearly neutralising the net biospheric CO_2 contribution (Fig. S12a). The overestimation of STILT simulations during October-November over Nainital can thus be due to the considerable overestimation of respiration fluxes or slight underestimation of carbon uptake from crops. Similarly, Mohali observations are influenced by the Rabi cultivation in Punjab and IGP, showing a decrease in CO_2 concentration during the December-January period, which the models do not represent well. Note that the VPRM ~~fluxes~~ model used in the ~~current STILT simulations are not calibrated with~~ present study lacks parameter optimisation against eddy-covariance flux observations across India. The availability of eddy-covariance flux observations representing various biomes in India is expected to improve model performance.

6.6 An assessment of usability of CO_2 observations in STILT-based inverse modelling

An accurate estimation of CO_2 fluxes through inverse modelling demands proper accountability of CO_2 variability by the forward model employed. The disagreements between the observations and simulations largely arise from an inadequate representation of mesoscale transport and local flux influences. Note that the STILT model can represent the seasonal variability at the observational sites (see Sect. 5.2) across India. Since improper accounting of CO_2 variability biases the inverse estimations, examining the systematic and unsystematic error terms (decoupled using Eq. (6) & (7), see Fig. 4) in STILT simulations is particularly relevant to assess the readiness of our models to utilise these measurements in the carbon assimilation system. Though it benefits the inverse modelling community, this study is not designed to entirely decouple the uncertainties solely due to inadequate transport and improper representation of flux variations in the model.

Figure 4a shows that the Mohali model-observation mismatch is more systematic (66-86 %) in nature. High $RMSE_s$ values are found over Mohali for most of the cases except for STILT-EGG4-ICOS simulations that utilised EGG4 products as initial & background condition and ICOS anthropogenic emission fluxes (Fig. 4a). These derived RMSE components and the higher percentage of systematic error contribution suggest further improvements in the models for potentially using Mohali data in inversion. The EGG4 product has higher spatiotemporal resolution compared to CarboScope, which may contribute to more realistic boundary conditions for the STILT simulation over Mohali. Similarly, the ICOS inventory is the only emission flux used in this study incorporating diurnal, weekly and monthly temporal variations. A reduced $RMSE_s$ (66 %) for models using the ICOS inventory suggests a need for representing temporal variations in emission fluxes for improved model performance at Mohali, where anthropogenic emissions play a significant role.

The $RMSE_s$ for STILT simulations over Nainital varies from 5.4 to 7.6 ppm, constituting about 52-60 % of the total RMSE. However, difficulty in capturing decreased CO_2 associated with the enhanced biospheric contribution in Nainital from August to December (more details in Sect. 6.5) indicates the inadequate representation of ecosystem uptake in the model. For instance, STILT-CS simulations could reproduce the observational variability from January to July with an $RMSE_s$ of $\sim$1.5 ppm. Besides

the growing period (August to December), the Nainital model-observation mismatch reports only 14 % of the systematic component in the total uncertainty (see Fig. S13). Similarly, Shadnagar and Nagpur simulations resulted in RMSE$_s$ of 1.6-3.6 ppm (4-34 % of total uncertainty) and 5.1-6.5 ppm (8-34 % of total uncertainty), respectively. The fact that the majority of the uncertainty in STILT simulations over Nainital, Shadnagar and Nagpur contributed by unsystematic components shows the ability of the STILT model to represent the CO_2 variability there. Hence, these observations can be utilised in inverse optimisation with the help of high-resolution simulations from STILT.

Noteworthy is that the RMSE$_s$ values are in general higher for reanalysis products compared to STILT simulations (Fig. 4), resulting in average values of 9.5 ppm, 10.4 ppm, 7.4 ppm and 11.1 ppm for Nainital, Shadnagar, Nagpur, and Mohali respectively. This indicates the advantage of using the STILT model over coarse-resolution models in utilizing these observations.

7   Conclusions

This study examines the potential of a high-resolution WRF-STILT modelling framework to simulate observed CO_2 variability over India. Further, we investigate the usability of these observations in inverse modelling when high-resolution models are used. Observations exhibit strong variability at seasonal (7.5-9.2 ppm) and intra-seasonal scales (2-12 ppm). To utilise these observations in inverse optimisations, the models need to address model-observation mismatches arising from fine-scale transport and local flux influences. Our model shows reasonable skill in representing the observed CO_2 variability in these stations, though the model could not sufficiently capture all the observed fine-scale variations. By improving fine-scale transport in the model, STILT simulations agree better with the observed seasonal and diurnal variations than the global reanalysis products. Among the reanalysis products, EGG4 products showed reasonable skill in predicting CO_2 variability over India.

Further, we explored the limitations of the STILT modelling system in representing the variability, although the model captures the intra-seasonal variabilities much better than the global models. However, the model must account for small-scale flux variations like biomass burning to represent Mohali observations. A considerable portion of these discrepancies can be ~~minimized~~ minimised by improving the prior emission flux distribution at high spatial and temporal scales. Both STILT and global models did not capture the sharp reduction of CO_2 concentration at Nainital during August, resulting from the increased biospheric uptake by the crops over the IGP region. ~~An improved estimate~~ In addition to using eddy-covariance flux observations in India, utilising additional satellite observations such as Solar Induced Fluorescence in the VPRM model can likely improve the prior representation of biospheric CO_2 uptake and release across Indian biomes (e.g., Ravi et al., 2023). Further, an improved (inverse) estimate of fluxes can be achieved by utilising ~~these~~ atmospheric CO_2 observations ~~to optimise the fluxes~~ through carbon data assimilation~~or by using flux observations from different ecosystems to calibrate the model parameters over India (e.g., Ravi et al., 2023)~~.

The extent of uncertainties in emission fluxes and their impact on CO_2 variations indicate the importance of improving the inventories and their proper representation in atmospheric transport modelling and inverse estimations. For instance, anthropogenic flux variability in CO_2 concentration dominates in Mohali, Shadnagar, and Nagpur due to their proximity to cities.

CO_{2ant} shows significant differences (up to 5 ppm) in their mean values and variability (up to 8 ppm) related to the choice of the emission inventory in the STILT model.

Except for Nainital, the observations used in the study are modulated by influences from local fluxes in addition to background variations. Hence, most of these observations are suitable for constraining carbon fluxes at local-to-urban scales. Nainital observations can be used in the regional carbon estimations as the observations showed significant influences from regional fluxes. Given the availability of high-resolution fluxes and better representation of the fine-scale transport, we demonstrate that the STILT can reasonably simulate the CO_2 variability over India. In other words, our study demonstrates a possible way of utilising observations from the Indian sub-continent that may potentially improve the global assimilation system estimates by increasing the degrees of freedom. Simultaneously, the availability of additional high-frequency observations representing the regional CO_2 variability over India, comparable to the World Meteorological Organization standards (https://gml.noaa.gov/ccl/co2_scale.html, last access: 12 June 2023) is necessary for improving the carbon estimates over India at scales relevant to policymaking.

Code and data availability.

The source code for WRF model version 3.9.1.1 that we used for the simulations of the meteorological fields is available from https://www2.mmm.ucar.edu/wrf/users/download/get_source.html (last access: 20 January 2022). STILT model source codes are available from https://stilt-model.org/ (last access: 15 March 2022). The EGG4 reanalysis products are availed from https://ads.atmosphere.copernicus.eu/cdsapp#!/dataset/cams-global-ghg-reanalysis-egg4?tab=form (last access: 10 February 2023). The CarboScope products used in this study are obtained from https://www.bgc-jena.mpg.de/CarboScope/ (last access: 20 July 2020). The CarbonTracker data is accessed from https://doi.org/10.25925/20201008 (last access: 22 October 2022). The EDGAR inventory data used in this study is from https://edgar.jrc.ec.europa.eu/dataset_ghg70 (last access: 19 January 2023). The ODIAC data is acquired from https://doi.org/10.17595/20170411.001 (last access: 23 February 2023). The ICOS data is obtained from https://hdl.handle.net/11676/-XUdi3MSHmJxSVBKmPmrTBOn (last access: 9 March 2022). GFAS data is downloaded from https://ads.atmosphere.copernicus.eu/cdsapp#!/dataset/cams-global-fire-emissions-gfas?tab=form(last access: 24 November 2021). The Fire Inventory from NCAR version 2.5 is accessed from https://rda.ucar.edu/datasets/ds312.9/dataaccess/ (last access: 3 July 2023). The Nanital CO_2 observations are obtained from https://doi.org/10.17595/20220301.001 (last access: 10 December 2022), and Shadnagar and Nagpur observations are downloaded from https://bhuvan-app3.nrsc.gov.in/data/download/index.php (last access: 12 December 2022). Additional materials, which contain the figures of some analysis for the manuscript, are available from https://zenodo.org/record/8143361 (last access: 13 July 2023, Thilakan and Pillai (2023)).

Author contributions.

DP conceptualized, and VT and DP designed the study. VT developed the analysis methods, and VT and JS conducted the model simulations. HH, VS, YT and MN made the CO_2 measurements. VT conducted the analyses and wrote the first draft of the manuscript. MD performed the satellite data acquisition and analysis. DP and CG supported the interpretation of the results. All authors discussed the results and provided feedback on the manuscript.

Competing interests.

At least one of the (co-)authors is a member of the editorial board of Atmospheric Chemistry and Physics.

Acknowledgements. This study has been supported by funding from the Max Planck Society allocated to the Max Planck Partner Group at IISERB. Vishnu Thilakan acknowledges the Ministry of Education (MoE) for his PhD funding. We acknowledge the support of IIS-ERB's high-performance computing facility for STILT model simulations and data analysis. The WRF simulations were done on the high-performance cluster system (Levante) of the German Climate Computing Center (DKRZ). We acknowledge the IISER Mohali Atmospheric Chemistry Facility funded by the Ministry of Education, India, for the data and thank current and previous members of the Atmospheric Chemistry and Emissions and Aerosol Research groups for technical assistance. The Nainital measurements were supported by the Environment Research and Technology Development Fund (JPMEERF20182002 and JPMEERF21S20802) of the Environmental Restoration and Conservation Agency of Japan, ARIES and ISRO-ATCTM project. We are thankful to Shohei Nomura, Toshinobu Machida, Motoki Sasakawa, Hitoshi Mukai and Deepak Chausali for making possible the Nainital measurements. We thank the Indian Space Research Organisation (ISRO)-Geosphere Biosphere Programme (ISRO-GBP) for providing free access to data. We also thank the Bhuvan/National Information System for Climate and Environment Studies (NICES) portal for providing the observations from Shadnagar and Nagpur, as well as Mahesh Pathakoti for technical support. We thank the editor, Abhishek Chatterjee, and referees (Sajeev Philip and the anonymous reviewer) for their constructive involvement in the review process.

References

Agustí-Panareda, A., Diamantakis, M., Massart, S., Chevallier, F., Muñoz Sabater, J., Barré, J., Curcoll, R., Engelen, R., Langerock, B., Law, R. M., Loh, Z., Morguí, J. A., Parrington, M., Peuch, V.-H., Ramonet, M., Roehl, C., Vermeulen, A. T., Warneke, T., and Wunch, D.: Modelling CO_2 weather – why horizontal resolution matters, Atmospheric Chemistry and Physics, 19, 7347–7376, https://doi.org/10.5194/acp-19-7347-2019, 2019.

Agustí-Panareda, A., Barré, J., Massart, S., Inness, A., Aben, I., Ades, M., Baier, B. C., Balsamo, G., Borsdorff, T., Bousserez, N., Boussetta, S., Buchwitz, M., Cantarello, L., Crevoisier, C., Engelen, R., Eskes, H., Flemming, J., Garrigues, S., Hasekamp, O., Huijnen, V., Jones, L., Kipling, Z., Langerock, B., McNorton, J., Meilhac, N., Noël, S., Parrington, M., Peuch, V.-H., Ramonet, M., Razinger, M., Reuter, M., Ribas, R., Suttie, M., Sweeney, C., Tarniewicz, J., and Wu, L.: Technical note: The CAMS greenhouse gas reanalysis from 2003 to 2020, Atmospheric Chemistry and Physics, 23, 3829–3859, https://doi.org/10.5194/acp-23-3829-2023, 2023.

Bhardwaj, P., Naja, M., Kumar, R., and Chandola, H. C.: Seasonal, interannual, and long-term variabilities in biomass burning activity over South Asia, Environmental Science and Pollution Research, 23, 4397–4410, https://doi.org/10.1007/s11356-015-5629-6, 2016.

Boadh, R., Satyanarayana, A., Rama Krishna, T., and Madala, S.: Sensitivity of PBL schemes of the WRF-ARW model in simulating the boundary layer flow parameters for their application to air pollution dispersion modeling over a tropical station, Atmósfera, 29, 61–81, https://doi.org/https://doi.org/10.20937/ATM.2016.29.01.05, 2016.

Broquet, G., Chevallier, F., Bréon, F.-M., Kadygrov, N., Alemanno, M., Apadula, F., Hammer, S., Haszpra, L., Meinhardt, F., Morguí, J. A., Necki, J., Piacentino, S., Ramonet, M., Schmidt, M., Thompson, R. L., Vermeulen, A. T., Yver, C., and Ciais, P.: Regional inversion of CO2 ecosystem fluxes from atmospheric measurements: reliability of the uncertainty estimates, Atmospheric Chemistry and Physics, 13, 9039–9056, https://doi.org/10.5194/acp-13-9039-2013, 2013.

CarboScope: Jena CarboScope Version s10oc_v2020, Max Planck Institute for Biogeochemistry [data set], http://www.bgc-jena.mpg.de/CarboScope/, last access: 20 July 2020, 2020.

Chandra, B., Sinha, V., Hakkim, H., and Sinha, B.: Storage stability studies and field application of low cost glass flasks for analyses of thirteen ambient VOCs using proton transfer reaction mass spectrometry, International Journal of Mass Spectrometry, 419, 11–19, https://doi.org/https://doi.org/10.1016/j.ijms.2017.05.008, 2017.

Chandra, N., Lal, S., Venkataramani, S., Patra, P. K., and Sheel, V.: Temporal variations of atmospheric CO_2 and CO at Ahmedabad in western India, Atmospheric Chemistry and Physics, 16, 6153–6173, https://doi.org/10.5194/acp-16-6153-2016, 2016.

Copernicus Atmosphere Monitoring Service: CAMS global greenhouse gas reanalysis (EGG4), CAMS Atmosphere Data Store (ADS) [data set], https://doi.org/10.24380/8fck-9w87, last access: 10 February 2023, 2021.

Crippa, M., Guizzardi, D., Muntean, M., Schaaf, E., Dentener, F., van Aardenne, J. A., Monni, S., Doering, U., Olivier, J. G. J., Pagliari, V., and Janssens-Maenhout, G.: Gridded emissions of air pollutants for the period 1970–2012 within EDGAR v4.3.2, Earth System Science Data, 10, 1987–2013, https://doi.org/10.5194/essd-10-1987-2018, 2018.

Crippa, M., Guizzardi, D., Banja, M., Solazzo, E., Muntean, M., Schaaf, E., Pagani, F., Monforti-Ferrario, F., Olivier, J., Quadrelli, R., Risquez Martin, A., Taghavi-Moharamli, P., Grassi, G., Rossi, S., Jacome Felix Oom, D., Branco, A., San-Miguel-Ayanz, J., and Vignati, E.: EDGAR (Emissions Database for Global Atmospheric Research) Community GHG Database (a collaboration between the European Commission, Joint Research Centre (JRC), the International Energy Agency (IEA), and comprising IEA-EDGAR CO2, EDGAR CH4, EDGAR N2O, EDGAR F-GASES version 7.0, European Commission, Joint Research Centre [data set], https://edgar.jrc.ec.europa.eu/dataset_ghg70, last access: 19 January 2023, 2022.

Deshpande, M. V., Kumar, N., Pillai, D., Krishna, V. V., and Jain, M.: Greenhouse gas emissions from agricultural residue burning have increased by 75% since 2011 across India, Science of The Total Environment, 904, 166 944, https://doi.org/https://doi.org/10.1016/j.scitotenv.2023.166944, 2023.

Enting, I. G.: Inverse Problems in Atmospheric Constituent Transport, Cambridge Atmospheric and Space Science Series, Cambridge University Press, https://doi.org/10.1017/CBO9780511535741, 2002.

Friedlingstein, P., O'Sullivan, M., Jones, M. W., Andrew, R. M., Gregor, L., Hauck, J., Le Quéré, C., Luijkx, I. T., Olsen, A., Peters, G. P., Peters, W., Pongratz, J., Schwingshackl, C., Sitch, S., Canadell, J. G., Ciais, P., Jackson, R. B., Alin, S. R., Alkama, R., Arneth, A., Aror a, V. K., Bates, N. R., Becker, M., Bellouin, N., Bittig, H. C., Bopp, L., Chevallier, F., Chini, L. P., Cronin, M., Evans, W., Falk, S., Feely, R. . A., Gasser, T., Gehlen, M., Gkritzalis, T., Gloege, L., Grassi, G., Gruber, N., Gürses, O., Harris, I., Hefner, M., Houghton, R. A., Hurtt, G. C., Iida, Y., Ilyina, T., Jain, A. K., Jersild, A., Kadono, K., Kato, E., Kennedy, D., Klein Goldewijk, K., Knauer, J., Korsbakken, J. I., Land schützer, P., Lefèvre, N., Lindsay, K., Liu, J., Liu, Z., Marland, G., Mayot, N., McGrath, M. J., Metzl, N., Monacci, N. M., Munro, D. R., Nak aoka, S.-I., Niwa, Y., O'Brien, K., Ono, T., Palmer, P. I., Pan, N., Pierrot, D., Pocock, K., Poulter, B., Resplandy, L., Robertson, E., Rödenbe ck, C., Rodriguez, C., Rosan, T. M., Schwinger, J., Séférian, R., Shutler, J. D., Skjelvan, I., Steinhoff, T., Sun, Q., Sutton, A. J., Sweeney, C. ., Takao, S., Tanhua, T., Tans, P. P., Tian, X., Tian, H., Tilbrook, B., Tsujino, H., Tubiello, F., van der Werf, G. R., Walker, A. P., Wanninkhof, R., Whitehead, C., Willstrand Wranne, A., Wright, R., Yuan, W., Yue, C., Yue, X., Zaehle, S., Zeng, J., and Zheng, B.: Global Carbon Budget 2022, Earth System Science Data, 14, 4811–4900, https://doi.org/10.5194/essd-14-4811-2022, 2022.

Ganesan, A. L., Rigby, M., Lunt, M. F., Parker, R. J., Boesch, H., Goulding, N., Umezawa, T., Zahn, A., Chatterjee, A., Prinn, R. G., Tiwari, Y. K., van der Schoot, M., and Krummel, P. B.: Atmospheric observations show accurate reporting and little growth in India's methane emissions, Nature Communications, 8, 836, https://doi.org/10.1038/s41467-017-00994-7, 2017.

Geels, C., Doney, S. C., Dargaville, R., Brandt, J., and Christensen, J. H.: Investigating the sources of synoptic variability in atmospheric CO2 measurements over the Northern Hemisphere continents: a regional model study, Tellus B: Chemical and Physical Meteorology, 56, 35–50, https://doi.org/10.3402/tellusb.v56i1.16399, 2004.

Geels, C., Gloor, M., Ciais, P., Bousquet, P., Peylin, P., Vermeulen, A. T., Dargaville, R., Aalto, T., Brandt, J., Christensen, J. H., Frohn, L. M., Haszpra, L., Karstens, U., Rödenbeck, C., Ramonet, M., Carboni, G., and Santaguida, R.: Comparing atmospheric transport models for future regional inversions over Europe - Part 1: mapping the atmospheric CO_2 signals, Atmospheric Chemistry and Physics, 7, 3461–3479, https://doi.org/10.5194/acp-7-3461-2007, 2007.

Gerbig, C., Lin, J. C., Wofsy, S. C., Daube, B. C., Andrews, A. E., Stephens, B. B., Bakwin, P. S., and Grainger, C. A.: Toward constraining regional-scale fluxes of CO2 with atmospheric observations over a continent: 2. Analysis of COBRA data using a receptor-oriented framework, Journal of Geophysical Research: Atmospheres, 108, https://doi.org/https://doi.org/10.1029/2003JD003770, 2003.

Gerbig, C., Körner, S., and Lin, J. C.: Vertical mixing in atmospheric tracer transport models: error characterization and propagation, Atmospheric Chemistry and Physics, 8, 591–602, https://doi.org/10.5194/acp-8-591-2008, 2008.

Gerbig, C., Dolman, A. J., and Heimann, M.: On observational and modelling strategies targeted at regional carbon exchange over continents, Biogeosciences, 6, 1949–1959, https://doi.org/10.5194/bg-6-1949-2009, 2009.

Halder, S., Tiwari, Y. K., Valsala, V., Sijikumar, S., Janardanan, R., and Maksyutov, S.: Benefits of satellite XCO2 and newly proposed atmospheric CO2 observation network over India in constraining regional CO2 fluxes, Science of The Total Environment, 812, 151 508, https://doi.org/https://doi.org/10.1016/j.scitotenv.2021.151508, 2022.

740 Hariprasad, K., Srinivas, C., Singh, A., Vijaya Bhaskara Rao, S., Baskaran, R., and Venkatraman, B.: Numerical simulation and intercomparison of boundary layer structure with different PBL schemes in WRF using experimental observations at a tropical site, Atmospheric Research, 145-146, 27–44, https://doi.org/https://doi.org/10.1016/j.atmosres.2014.03.023, 2014.

Houweling, S., Aben, I., Breon, F.-M., Chevallier, F., Deutscher, N., Engelen, R., Gerbig, C., Griffith, D., Hungershoefer, K., Macatangay, R., Marshall, J., Notholt, J., Peters, W., and Serrar, S.: The importance of transport model uncertainties for the estimation of CO_2 sources
745 and sinks using satellite measurements, Atmospheric Chemistry and Physics, 10, 9981–9992, https://doi.org/10.5194/acp-10-9981-2010, 2010.

Inness, A., Ades, M., Agustí-Panareda, A., Barré, J., Benedictow, A., Blechschmidt, A.-M., Dominguez, J. J., Engelen, R., Eskes, H., Flemming, J., Huijnen, V., Jones, L., Kipling, Z., Massart, S., Parrington, M., Peuch, V.-H., Razinger, M., Remy, S., Schulz, M., and Suttie, M.: The CAMS reanalysis of atmospheric composition, Atmospheric Chemistry and Physics, 19, 3515–3556, https://doi.org/10.5194/acp-19-
750 3515-2019, 2019.

Jacobson, A. R., Schuldt, K. N., Miller, J. B., Oda, T., Tans, P., Arlyn Andrews, Mund, J., Ott, L., Collatz, G. J., Aalto, T., Afshar, S., Aikin, K., Aoki, S., Apadula, F., Baier, B., Bergamaschi, P., Beyersdorf, A., Biraud, S. C., Bollenbacher, A., Bowling, D., Brailsford, G., Abshire, J. B., Chen, G., Huilin Chen, Lukasz Chmura, Sites Climadat, Colomb, A., Conil, S., Cox, A., Cristofanelli, P., Cuevas, E., Curcoll, R., Sloop, C. D., Davis, K., Wekker, S. D., Delmotte, M., DiGangi, J. P., Dlugokencky, E., Ehleringer, J., Elkins, J. W., Emmenegger, L.,
755 Fischer, M. L., Forster, G., Frumau, A., Galkowski, M., Gatti, L. V., Gloor, E., Griffis, T., Hammer, S., Haszpra, L., Hatakka, J., Heliasz, M., Hensen, A., Hermanssen, O., Hintsa, E., Holst, J., Jaffe, D., Karion, A., Kawa, S. R., Keeling, R., Keronen, P., Kolari, P., Kominkova, K., Kort, E., Krummel, P., Kubistin, D., Labuschagne, C., Langenfelds, R., Laurent, O., Laurila, T., Lauvaux, T., Law, B., Lee, J., Lehner, I., Leuenberger, M., Levin, I., Levula, J., Lin, J., Lindauer, M., Loh, Z., Lopez, M., Luijkx, I. T., Myhre, C. L., Machida, T., Mammarella, I., Manca, G., Manning, A., Manning, A., Marek, M. V., Marklund, P., Martin, M. Y., Matsueda, H., McKain, K., Meijer, H., Meinhardt, F.,
760 Miles, N., Miller, C. E., Mölder, M., Montzka, S., Moore, F., Josep-Anton Morgui, Morimoto, S., Munger, B., Jaroslaw Necki, Newman, S., Nichol, S., Niwa, Y., O'Doherty, S., Mikaell Ottosson-Löfvenius, Paplawsky, B., Peischl, J., Peltola, O., Jean-Marc Pichon, Piper, S., Plass-Dölmer, C., Ramonet, M., Reyes-Sanchez, E., Richardson, S., Riris, H., Ryerson, T., Saito, K., Sargent, M., Sasakawa, M., Sawa, Y., Say, D., Scheeren, B., Schmidt, M., Schmidt, A., Schumacher, M., Shepson, P., Shook, M., Stanley, K., Steinbacher, M., Stephens, B., Sweeney, C., Thoning, K., Torn, M., Turnbull, J., Tørseth, K., Bulk, P. V. D., Dinther, D. V., Vermeulen, A., Viner, B., Vitkova, G., Walker,
765 S., Weyrauch, D., Wofsy, S., Worthy, D., Dickon Young, and Miroslaw Zimnoch: CarbonTracker CT2019B, NOAA Global Monitoring Laboratory [data set], https://doi.org/10.25925/20201008, 2020.

Jain, C. D., Singh, V., Akhil Raj, S., Madhavan, B., and Ratnam, M. V.: Local emission and long-range transport impacts on the CO, CO2, and CH4 concentrations at a tropical rural site, Atmospheric Environment, 254, 118 397, https://doi.org/https://doi.org/10.1016/j.atmosenv.2021.118397, 2021.

770 Janssens-Maenhout, G., Crippa, M., Guizzardi, D., Muntean, M., Schaaf, E., Dentener, F., Bergamaschi, P., Pagliari, V., Olivier, J. G. J., Peters, J. A. H. W., van Aardenne, J. A., Monni, S., Doering, U., Petrescu, A. M. R., Solazzo, E., and Oreggioni, G. D.: EDGAR v4.3.2 Global Atlas of the three major greenhouse gas emissions for the period 1970–2012, Earth System Science Data, 11, 959–1002, https://doi.org/10.5194/essd-11-959-2019, 2019.

Kaiser, J. W., Heil, A., Andreae, M. O., Benedetti, A., Chubarova, N., Jones, L., Morcrette, J.-J., Razinger, M., Schultz, M. G., Suttie, M.,
775 and van der Werf, G. R.: Biomass burning emissions estimated with a global fire assimilation system based on observed fire radiative power, Biogeosciences, 9, 527–554, https://doi.org/10.5194/bg-9-527-2012, 2012.

Karstens, U., Gerbig, C., and Janssens-Maenhout, G.: Global anthropogenic CO2 emissions based on EDGARv4.3 and BP statistics 2019, Carbon Portal [data set], https://hdl.handle.net/11676/-XUdi3MSHmJxSVBKmPmrTBOn, last access: 9 March 2022, 2019.

Kompalli, S. K., Babu, S. S., Moorthy, K. K., Manoj, M., Kumar, N. K., Shaeb, K. H. B., and Joshi, A. K.: Aerosol black carbon characteristics over Central India: Temporal variation and its dependence on mixed layer height, Atmospheric Research, 147-148, 27–37, https://doi.org/https://doi.org/10.1016/j.atmosres.2014.04.015, 2014.

Kumar, R., Naja, M., Satheesh, S. K., Ojha, N., Joshi, H., Sarangi, T., Pant, P., Dumka, U. C., Hegde, P., and Venkataramani, S.: Influences of the springtime northern Indian biomass burning over the central Himalayas, Journal of Geophysical Research: Atmospheres, 116, https://doi.org/https://doi.org/10.1029/2010JD015509, 2011.

Kumar, V. and Sinha, V.: Season-wise analyses of VOCs, hydroxyl radicals and ozone formation chemistry over north-west India reveal isoprene and acetaldehyde as the most potent ozone precursors throughout the year, Chemosphere, 283, 131 184, https://doi.org/https://doi.org/10.1016/j.chemosphere.2021.131184, 2021.

Lauvaux, T., Uliasz, M., Sarrat, C., Chevallier, F., Bousquet, P., Lac, C., Davis, K. J., Ciais, P., Denning, A. S., and Rayner, P. J.: Mesoscale inversion: first results from the CERES campaign with synthetic data, Atmospheric Chemistry and Physics, 8, 3459–3471, https://doi.org/10.5194/acp-8-3459-2008, 2008.

Law, R. M., Rayner, P. J., Steele, L. P., and Enting, I. G.: Using high temporal frequency data for CO2 inversions, Global Biogeochemical Cycles, 16, 1–1–1–18, https://doi.org/https://doi.org/10.1029/2001GB001593, 2002.

Lin, J. C., Gerbig, C., Wofsy, S. C., Andrews, A. E., Daube, B. C., Davis, K. J., and Grainger, C. A.: A near-field tool for simulating the upstream influence of atmospheric observations: The Stochastic Time-Inverted Lagrangian Transport (STILT) model, Journal of Geophysical Research: Atmospheres, 108, https://doi.org/https://doi.org/10.1029/2002JD003161, 2003.

Lin, J. C., Gerbig, C., Wofsy, S. C., Andrews, A. E., Daube, B. C., Grainger, C. A., Stephens, B. B., Bakwin, P. S., and Hollinger, D. Y.: Measuring fluxes of trace gases at regional scales by Lagrangian observations: Application to the CO2 Budget and Rectification Airborne (COBRA) study, Journal of Geophysical Research: Atmospheres, 109, https://doi.org/https://doi.org/10.1029/2004JD004754, 2004.

Lin, X., Indira, N. K., Ramonet, M., Delmotte, M., Ciais, P., Bhatt, B. C., Reddy, M. V., Angchuk, D., Balakrishnan, S., Jorphail, S., Dorjai, T., Mahey, T. T., Patnaik, S., Begum, M., Brenninkmeijer, C., Durairaj, S., Kirubagaran, R., Schmidt, M., Swathi, P. S., Vinithkumar, N. V., Yver Kwok, C., and Gaur, V. K.: Long-lived atmospheric trace gases measurements in flask samples from three stations in India, Atmospheric Chemistry and Physics, 15, 9819–9849, https://doi.org/10.5194/acp-15-9819-2015, 2015.

Mahadevan, P., Wofsy, S. C., Matross, D. M., Xiao, X., Dunn, A. L., Lin, J. C., Gerbig, C., Munger, J. W., Chow, V. Y., and Gottlieb, E. W.: A satellite-based biosphere parameterization for net ecosystem CO2 exchange: Vegetation Photosynthesis and Respiration Model (VPRM), Global Biogeochemical Cycles, 22, https://doi.org/https://doi.org/10.1029/2006GB002735, 2008.

Mahesh, P., Sreenivas, G., Rao, P., Dadhwal, V., Krishna, S. S., and Mallikarjun, K.: High-precision surface-level CO2 and CH4 using off-axis integrated cavity output spectroscopy (OA-ICOS) over Shadnagar, India, International Journal of Remote Sensing, 36, 5754–5765, https://doi.org/10.1080/01431161.2015.1104744, 2015.

Maier, F., Gerbig, C., Levin, I., Super, I., Marshall, J., and Hammer, S.: Effects of point source emission heights in WRF–STILT: a step towards exploiting nocturnal observations in models, Geoscientific Model Development, 15, 5391–5406, https://doi.org/10.5194/gmd-15-5391-2022, 2022.

Mathew, T. A., Ravi, A., Pillai, D., Saradambal, L., Kumar, J. S., Gopalakrishnan, M. M., and Thilakan, V.: Evaluating the meteorological transport model ensemble for accounting uncertainties in carbon flux estimation over India, EGUsphere, 2024, 1–35, https://doi.org/10.5194/egusphere-2023-2334, 2024.

815 MODIS-FIRMS: MODIS Collection 61 NRT Hotspot / Active Fire Detections MCD14DL distributed from NASA FIRMS [data set], https://doi.org/10.5067/FIRMS/MODIS/MCD14DL.NRT.0061, last access: 25 June 2023, 2021.

Nehrkorn, T., Eluszkiewicz, J., Wofsy, S. C., Lin, J. C., Gerbig, C., Longo, M., and Freitas, S.: Coupled weather research and forecasting–stochastic time-inverted lagrangian transport (WRF–STILT) model, Meteorology and Atmospheric Physics, 107, 51–64, https://doi.org/10.1007/s00703-010-0068-x, 2010.

820 Nomura, S., Naja, M., Ahmed, M. K., Mukai, H., Terao, Y., Machida, T., Sasakawa, M., and Patra, P. K.: Measurement report: Regional characteristics of seasonal and long-term variations in greenhouse gases at Nainital, India, and Comilla, Bangladesh, Atmospheric Chemistry and Physics, 21, 16 427–16 452, https://doi.org/10.5194/acp-21-16427-2021, 2021.

Oda, T. and Maksyutov, S.: ODIAC Fossil Fuel CO_2 Emissions Dataset (Version name : ODIAC2020), Center for Global Environmental Research, National Institute for Environmental Studies [data set], https://doi.org/10.17595/20170411.001, last access: 23 February 2023, 825 2020.

Oda, T., Maksyutov, S., and Andres, R. J.: The Open-source Data Inventory for Anthropogenic CO_2, version 2016 (ODIAC2016): a global monthly fossil fuel CO_2 gridded emissions data product for tracer transport simulations and surface flux inversions, Earth System Science Data, 10, 87–107, https://doi.org/10.5194/essd-10-87-2018, 2018.

Patra, P. K., Canadell, J. G., Houghton, R. A., Piao, S. L., Oh, N.-H., Ciais, P., Manjunath, K. R., Chhabra, A., Wang, T., Bhattacharya, T., 830 Bousquet, P., Hartman, J., Ito, A., Mayorga, E., Niwa, Y., Raymond, P. A., Sarma, V. V. S. S., and Lasco, R.: The carbon budget of South Asia, Biogeosciences, 10, 513–527, https://doi.org/10.5194/bg-10-513-2013, 2013.

Pawar, H., Garg, S., Kumar, V., Sachan, H., Arya, R., Sarkar, C., Chandra, B. P., and Sinha, B.: Quantifying the contribution of long-range transport to particulate matter (PM) mass loadings at a suburban site in the north-western Indo-Gangetic Plain (NW-IGP), Atmospheric Chemistry and Physics, 15, 9501–9520, https://doi.org/10.5194/acp-15-9501-2015, 2015.

835 Peters, W., Jacobson, A. R., Sweeney, C., Andrews, A. E., Conway, T. J., Masarie, K., Miller, J. B., Bruhwiler, L. M. P., Petron, G., Hirsch, A. I., Worthy, D. E. J., van der Werf, G. R., Randerson, J. T., Wennberg, P. O., Krol, M. C., and Tans, P. P.: An atmospheric perspective on North American carbon dioxide exchange: CarbonTracker, Proceedings of the National Academy of Sciences, 104, 18 925–18 930, https://doi.org/10.1073/pnas.0708986104, 2007.

Philip, S., Johnson, M. S., Baker, D. F., Basu, S., Tiwari, Y. K., Indira, N. K., Ramonet, M., and Poulter, B.: OCO-2 Satellite-Imposed 840 Constraints on Terrestrial Biospheric CO2 Fluxes Over South Asia, Journal of Geophysical Research: Atmospheres, 127, e2021JD035 035, https://doi.org/https://doi.org/10.1029/2021JD035035, e2021JD035035 2021JD035035, 2022.

Pillai, D., Gerbig, C., Ahmadov, R., Rödenbeck, C., Kretschmer, R., Koch, T., Thompson, R., Neininger, B., and Lavrié, J. V.: High-resolution simulations of atmospheric CO_2 over complex terrain – representing the Ochsenkopf mountain tall tower, Atmospheric Chemistry and Physics, 11, 7445–7464, https://doi.org/10.5194/acp-11-7445-2011, 2011.

845 Pillai, D., Buchwitz, M., Gerbig, C., Koch, T., Reuter, M., Bovensmann, H., Marshall, J., and Burrows, J. P.: Tracking city CO_2 emissions from space using a high-resolution inverse modelling approach: a case study for Berlin, Germany, Atmospheric Chemistry and Physics, 16, 9591–9610, https://doi.org/10.5194/acp-16-9591-2016, 2016.

Ravi, A., Pillai, D., Gerbig, C., Sitch, S., Zaehle, S., Thilakan, V., and Jha, C. S.: Spatiotemporal variations in terrestrial biospheric CO_2 fluxes of India derived from MODIS, OCO-2 and TROPOMI satellite observations and a diagnostic terrestrial vegetation model, EGUsphere, 850 2023, 1–69, https://doi.org/10.5194/egusphere-2023-817, 2023.

Ravindra, K., Singh, T., and Mor, S.: COVID-19 pandemic and sudden rise in crop residue burning in India: issues and prospects for sustainable crop residue management, Environmental Science and Pollution Research, 29, 3155–3161, https://doi.org/10.1007/s11356-021-17550-y, 2022.

Rödenbeck, C., Houweling, S., Gloor, M., and Heimann, M.: CO_2 flux history 1982–2001 inferred from atmospheric data using a global
855   inversion of atmospheric transport, Atmospheric Chemistry and Physics, 3, 1919–1964, https://doi.org/10.5194/acp-3-1919-2003, 2003.

Sahu, S. K., Mangaraj, P., Beig, G., Samal, A., Chinmay Pradhan, Dash, S., and Tyagi, B.: Quantifying the high resolution seasonal emission of air pollutants from crop residue burning in India, Environmental Pollution, 286, 117 165, https://doi.org/https://doi.org/10.1016/j.envpol.2021.117165, 2021.

Sarangi, T., Naja, M., Ojha, N., Kumar, R., Lal, S., Venkataramani, S., Kumar, A., Sagar, R., and Chandola, H. C.: First simultaneous
860   measurements of ozone, CO, and NOy at a high-altitude regional representative site in the central Himalayas, Journal of Geophysical Research: Atmospheres, 119, 1592–1611, https://doi.org/https://doi.org/10.1002/2013JD020631, 2014.

Schuh, A. E., Jacobson, A. R., Basu, S., Weir, B., Baker, D., Bowman, K., Chevallier, F., Crowell, S., Davis, K. J., Deng, F., Denning, S., Feng, L., Jones, D., Liu, J., and Palmer, P. I.: Quantifying the Impact of Atmospheric Transport Uncertainty on CO2 Surface Flux Estimates, Global Biogeochemical Cycles, 33, 484–500, https://doi.org/https://doi.org/10.1029/2018GB006086, 2019.

865 Shaeb, K. H. B., Rao, K. K., and Althaf, P.: Seasonal Characteristics of Black Carbon Aerosols over an Urban City in India: Source Analysis Using Concentration Weighted Trajectories, Asia-Pacific Journal of Atmospheric Sciences, 56, 29–43, https://doi.org/10.1007/s13143-019-00126-9, 2020.

Sijikumar, S., Raju, A., Valsala, V., Tiwari, Y., Girach, I., Jain, C. D., and Ratnam, M. V.: High-Resolution Bayesian Inversion of Carbon Dioxide Flux Over Peninsular India, Atmospheric Environment, 308, 119 868,
870   https://doi.org/https://doi.org/10.1016/j.atmosenv.2023.119868, 2023.

Sinha, V., Kumar, V., and Sarkar, C.: Chemical composition of pre-monsoon air in the Indo-Gangetic Plain measured using a new air quality facility and PTR-MS: high surface ozone and strong influence of biomass burning, Atmospheric Chemistry and Physics, 14, 5921–5941, https://doi.org/10.5194/acp-14-5921-2014, 2014.

Sivan, C., Rakesh, V., Abhilash, S., and Mohanakumar, K.: Evaluation of global reanalysis winds and high-resolution regional model outputs
875   with the 205 MHz stratosphere–troposphere wind profiler radar observations, Quarterly Journal of the Royal Meteorological Society, 147, 2562–2579, https://doi.org/https://doi.org/10.1002/qj.4041, 2021.

Sreenivas, G., Mahesh, P., Subin, J., Kanchana, A. L., Rao, P. V. N., and Dadhwal, V. K.: Influence of Meteorology and interrelationship with greenhouse gases (CO_2 and CH_4) at a suburban site of India, Atmospheric Chemistry and Physics, 16, 3953–3967, https://doi.org/10.5194/acp-16-3953-2016, 2016.

880 Stein, A. F., Draxler, R. R., Rolph, G. D., Stunder, B. J. B., Cohen, M. D., and Ngan, F.: NOAA's HYSPLIT Atmospheric Transport and Dispersion Modeling System, Bulletin of the American Meteorological Society, 96, 2059 – 2077, https://doi.org/https://doi.org/10.1175/BAMS-D-14-00110.1, 2015.

Terao, Y., Nomura, S., Mukai, H., Machida, T., Sasakawa, M., and Naja, M.: Atmospheric Carbon Dioxide Dry Air Mole Fraction at Nainital, India, ver.2022.0 [data set], https://doi.org/10.17595/20220301.001, last access: 10 December 2022, 2022.

885 Thilakan, V. and Pillai, D.: Additional Materials for "Potential of using CO2 observations over India in regional carbon budget estimation by improving the modelling system", https://doi.org/10.5281/zenodo.8143361, last access: 13 July 2023, 2023.

Thilakan, V., Pillai, D., Gerbig, C., Galkowski, M., Ravi, A., and Anna Mathew, T.: Towards monitoring the CO_2 source–sink distribution over India via inverse modelling: quantifying the fine-scale spatiotemporal variability in the atmospheric CO_2 mole fraction, Atmospheric Chemistry and Physics, 22, 15 287–15 312, https://doi.org/10.5194/acp-22-15287-2022, 2022.

890 Thompson, R. L., Ishijima, K., Saikawa, E., Corazza, M., Karstens, U., Patra, P. K., Bergamaschi, P., Chevallier, F., Dlugokencky, E., Prinn, R. G., Weiss, R. F., O'Doherty, S., Fraser, P. J., Steele, L. P., Krummel, P. B., Vermeulen, A., Tohjima, Y., Jordan, A., Haszpra, L., Steinbacher, M., Van der Laan, S., Aalto, T., Meinhardt, F., Popa, M. E., Moncrieff, J., and Bousquet, P.: TransCom N_2O model inter-comparison – Part 2: Atmospheric inversion estimates of N_2O emissions, Atmospheric Chemistry and Physics, 14, 6177–6194, https://doi.org/10.5194/acp-14-6177-2014, 2014.

895 Thompson, R. L., Patra, P. K., Chevallier, F., Maksyutov, S., Law, R. M., Ziehn, T., van der Laan-Luijkx, I. T., Peters, W., Ganshin, A., Zhuravlev, R., Maki, T., Nakamura, T., Shirai, T., Ishizawa, M., Saeki, T., Machida, T., Poulter, B., Canadell, J. G., and Ciais, P.: Top–down assessment of the Asian carbon budget since the mid 1990s, Nature Communications, 7, 10 724, https://doi.org/10.1038/ncomms10724, 2016.

Tiwari, Y. K., Vellore, R. K., Ravi Kumar, K., van der Schoot, M., and Cho, C.-H.: Influence of monsoons on atmo-
900 spheric CO2 spatial variability and ground-based monitoring over India, Science of The Total Environment, 490, 570–578, https://doi.org/https://doi.org/10.1016/j.scitotenv.2014.05.045, 2014.

Tolk, L. F., Meesters, A. G. C. A., Dolman, A. J., and Peters, W.: Modelling representation errors of atmospheric CO_2 mixing ratios at a regional scale, Atmospheric Chemistry and Physics, 8, 6587–6596, https://doi.org/10.5194/acp-8-6587-2008, 2008.

Umezawa, T., Niwa, Y., Sawa, Y., Machida, T., and Matsueda, H.: Winter crop CO2 uptake inferred from CONTRAIL measurements over
905 Delhi, India, Geophysical Research Letters, 43, 11,859–11,866, https://doi.org/https://doi.org/10.1002/2016GL070939, 2016.

Vellalassery, A., Pillai, D., Marshall, J., Gerbig, C., Buchwitz, M., Schneising, O., and Ravi, A.: Using TROPOspheric Monitoring Instrument (TROPOMI) measurements and Weather Research and Forecasting (WRF) CO modelling to understand the contribution of meteorology and emissions to an extreme air pollution event in India, Atmospheric Chemistry and Physics, 21, 5393–5414, https://doi.org/10.5194/acp-21-5393-2021, 2021.

910 Vogelezang, D. H. P. and Holtslag, A. A. M.: Evaluation and model impacts of alternative boundary-layer height formulations, Boundary-Layer Meteorology, 81, 245–269, https://doi.org/10.1007/BF02430331, 1996.

Wiedinmyer, C. and Emmons, L.: Fire Inventory from NCAR version 2 Fire Emission, https://doi.org/10.5065/XNPA-AF09, 2022.

Wiedinmyer, C., Kimura, Y., McDonald-Buller, E. C., Emmons, L. K., Buchholz, R. R., Tang, W., Seto, K., Joseph, M. B., Barsanti, K. C., Carlton, A. G., and Yokelson, R.: The Fire Inventory from NCAR version 2.5: an updated global fire emissions model for climate and
915 chemistry applications, EGUsphere, 2023, 1–45, https://doi.org/10.5194/egusphere-2023-124, 2023.

Willmott, C. J.: ON THE VALIDATION OF MODELS, Physical Geography, 2, 184–194, https://doi.org/10.1080/02723646.1981.10642213, 1981.

Willmott, C. J., Robeson, S. M., and Matsuura, K.: A refined index of model performance, International Journal of Climatology, 32, 2088–2094, https://doi.org/https://doi.org/10.1002/joc.2419, 2012.